



THE UNIVERSITY *of* EDINBURGH

Edinburgh Research Explorer

Identifying areas at risk of drought-induced tree mortality across South-Eastern Australia

Citation for published version:

De Kauwe, MG, Medlyn, BE, Ukkola, AM, Ukkola, AM, Mu, M, Sabot, MEB, Pitman, AJ, Meir, P, Cernusak, LA, Rifai, SW, Choat, B, Tissue, DT, Blackman, CJ, Li, X, Roderick, M & Briggs, PR 2020, 'Identifying areas at risk of drought-induced tree mortality across South-Eastern Australia', *Global Change Biology*.
<https://doi.org/10.1111/gcb.15215>

Digital Object Identifier (DOI):

[10.1111/gcb.15215](https://doi.org/10.1111/gcb.15215)

Link:

[Link to publication record in Edinburgh Research Explorer](#)

Document Version:

Peer reviewed version

Published In:

Global Change Biology

General rights

Copyright for the publications made accessible via the Edinburgh Research Explorer is retained by the author(s) and / or other copyright owners and it is a condition of accessing these publications that users recognise and abide by the legal requirements associated with these rights.

Take down policy

The University of Edinburgh has made every reasonable effort to ensure that Edinburgh Research Explorer content complies with UK legislation. If you believe that the public display of this file breaches copyright please contact openaccess@ed.ac.uk providing details, and we will remove access to the work immediately and investigate your claim.



1 **Identifying areas at risk of drought-induced tree mortality across South-**

2 **Eastern Australia**

3 Martin G. De Kauwe^{1,2,3*}, Belinda E. Medlyn⁴, Anna M. Ukkola^{1,5}, Mengyuan Mu^{1,2}, Manon
4 E. B. Sabot^{1,2}, Andrew J. Pitman^{1,2}, Patrick Meir^{6,7}, Lucas Cernusak⁸, Sami W. Rifai², B.
5 Choat⁴, David T. Tissue⁴, Chris J. Blackman⁴, Ximeng Li⁴, Michael Roderick^{1,5} and Peter R.
6 Briggs⁹.

7 ¹ARC Centre of Excellence for Climate Extremes, Sydney, NSW 2052, Australia.

8 ²Climate Change Research Centre, University of New South Wales, Sydney, NSW 2052,
9 Australia.

10 ³Evolution & Ecology Research Centre, University of New South Wales, Sydney, NSW
11 2052, Australia.

12 ⁴Hawkesbury Institute for the Environment, Western Sydney University, Locked Bag 1797,
13 Penrith, NSW 2751, Australia

14 ⁵Research School of Earth Sciences, Australian National University, Canberra, ACT 2601,
15 Australia

16 ⁶Research School of Biology, The Australian National University, Acton ACT 2601,
17 Australia

18 ⁷School of Geosciences, University of Edinburgh, Edinburgh EH93ff United Kingdom

19 ⁸College of Science and Engineering, James Cook University, Cairns, Qld 4814, Australia

20 ⁹CSIRO Oceans and Atmosphere, Canberra, 2601, Australia

21 * *Corresponding author address*: Martin De Kauwe, Climate Change Research Centre,
22 University of New South Wales, New South Wales 2052, Australia. E-mail:
23 mdekauwe@gmail.com Phone: +61 2 9385 8481

24 Running head: *Predicting drought-induced tree mortality* Keywords: *cavitation resistance,*
25 *drought tolerance, plant hydraulics, land surface model, Australia*

26 Keywords:

26 Word count: 8143/8000

27

28 **Abstract**

29 South-East Australia has recently been subjected to two of the worst droughts in the historical
30 record (Millennium Drought, 2000–2009 and Big Dry, 2017–2019). Unfortunately, a lack of
31 forest monitoring has made it difficult to determine whether widespread tree mortality has
32 resulted from these droughts. Anecdotal observations suggest the Big Dry may have led to
33 more significant tree mortality than the Millennium drought. Critically, to be able to robustly
34 project future expected climate change effects on Australian vegetation, we need to be able to
35 assess the vulnerability to drought of Australian trees. Here, we implemented a model of plant
36 hydraulics into the Community Atmosphere Biosphere Land Exchange (CABLE) land surface
37 model. We parameterised the drought response behaviour of five broad vegetation types,
38 based on a common garden dry-down experiment with species originating across a rainfall
39 gradient (188–1125 mm yr⁻¹) across South-East Australia. The new hydraulics model

40 significantly improved (~35–45 % reduction in root mean square error) CABLE's previous
41 predictions of latent heat fluxes during periods of water stress at two eddy covariance sites in
42 Australia. Landscape-scale predictions of the greatest percentage loss of hydraulic
43 conductivity (PLC), 40–60 %, were broadly consistent with satellite estimates of regions of
44 the greatest change in both droughts. In neither drought did CABLE predict that trees would
45 have reached critical PLC in widespread areas (i.e. it projected a low mortality risk), although
46 the model highlighted critical levels near the desert regions of South-East Australia where few
47 trees live. Overall, our experimentally constrained model results imply significant resilience
48 to drought conferred by hydraulic function, but also highlight critical data and scientific gaps.
49 Our approach presents a promising avenue to integrate experimental data and make regional-
50 scale predictions of potential drought-induced hydraulic failure.

51 **Introduction**

52 Australia is the driest inhabited continent, with the greatest inter-annual variability in rainfall,
53 and is prone to severe multi-year droughts. Tree species that occur in this environment are
54 well adapted to rainfall variability and extended drought periods (Myers & Neales, 1984;
55 Stoneman, 1994; Arndt *et al.*, 2015), but it is nonetheless unclear whether they will continue
56 to thrive as the climate changes. Some climate studies project more intense, longer lasting and
57 more frequent droughts (Dai, 2013; Trenberth *et al.*, 2014; Cook *et al.*, 2015), although
58 divergence in model projections of future regional precipitation patterns (Collins *et al.*, 2013)
59 makes it difficult to determine how drought characteristics may change. Nevertheless, we can
60 be certain that future drought episodes will occur against the widely predicted background of
61 increasing air temperature in the immediate future (Reichstein *et al.*, 2013; Williams *et al.*,
62 2013; Trenberth *et al.*, 2014). Globally, projected changes in drought incidence are consistent
63 with increased reports of severe drought events (Ciais *et al.*, 2005; Fensham *et al.*, 2009;

64 Phillips *et al.*, 2009; Allen *et al.*, 2015), declines in forest productivity linked to water
65 limitations (Peñuelas *et al.*, 2011) and associated tree mortality (Breshears *et al.*, 2005;
66 Anderegg *et al.*, 2013; Mitchell *et al.*, 2014).

67 In contrast to the apparent increasing global trend in drought-induced tree mortality, there
68 have been relatively few reports of similar events in Australia. Mitchell *et al.* (2014) in their
69 literature review found only 17 scientific reports of drought-related die-off events since 1891.
70 The decadal (2000–2010) Millennium drought was the worst drought on record for South-
71 East Australia (van Dijk *et al.*, 2013); Figures S1 and S2) and yet, Jiang *et al.* (2019),
72 attempting to ground-truth remotely-sensed drought impacts, found only four locations where
73 drought mortality was observed during the period. However, archival studies of newspaper
74 reports during historical droughts, such as the Federation Drought (1891-1903), have found
75 numerous observations of drought-related mortality (Fensham & Holman, 1999; Godfree *et*
76 *al.*, 2019). This poses an important question: is widespread drought-induced mortality rare
77 among Australian trees? Or simply under-reported?

78 Despite detailed reporting on the impacts of the Millennium drought on agriculture,
79 hydrology and the economy (Carter & White, 2009; van Dijk *et al.*, 2013), there remains a
80 striking gap in the quantification of drought impacts for Australia's tree species. This critical
81 knowledge gap means that we do not know which species or forest types are most vulnerable,
82 or what thresholds of drought stress are required to induce tree mortality among Australian
83 species. Without this information, we are limited in our ability to develop or test a
84 physiological understanding of the mechanisms that lead to tree die-off. As a result, we
85 cannot robustly predict future drought vulnerability for Australian trees or predict changes in
86 community species composition due to drought (Mueller *et al.*, 2005; Nepstad *et al.*, 2007;
87 Ruthrof *et al.*, 2015). A better understanding of the required magnitude of water stress that

88 would invoke hydraulic failure and lead to mortality (Adams *et al.*, 2017) is urgently needed
89 to comprehend the drought-tolerance of tree species, both within Australia and across the
90 globe.

91 Based on current literature, it is unclear whether species occurring in mesic or xeric
92 environments are most vulnerable to the impacts of drought, or if both environments are
93 equally vulnerable (Choat *et al.*, 2012). We might hypothesise that species growing in more
94 arid environments would be well adapted to water stress (i.e. greater xylem resilience to
95 cavitation). By contrast, in mesic regions, climate variability is typically muted. As a result,
96 ecological adaptations may be less plastic to stochastic drought (Arndt *et al.*, 2015; Jump *et al.*,
97 2017), as witnessed in the large Amazon rainforest droughts (Bittencourt *et al.*, 2020).
98 Similarly, many studies have highlighted a greater drought sensitivity in larger trees,
99 especially in particular taxa (Nepstad *et al.*, 2007; Phillips *et al.*, 2010; Rowland *et al.*, 2015;
100 Bittencourt *et al.*, 2020), consistent with a hypothesis of greater drought stress in mesic
101 species via the water transport system. Conversely, other studies have shown greater impacts
102 of drought in drier environments (Ruiz-Benito *et al.*, 2014; Anderegg *et al.*, 2015), or for
103 species growing at the edge of their distributions (Galiano *et al.*, 2010; Anderegg *et al.*, 2019).
104 Many taller trees could also have invested more heavily in a deeper rooting structure (Fan *et*
105 *al.*, 2017), which implies resilience may be at odds with apparent greater drought sensitivity.
106 Overall, there is no clear consensus among studies as to where, when, and which species are
107 most vulnerable to the impacts of drought

108 One way to estimate drought mortality thresholds is to use empirical approaches based on
109 mortality observations. In the southwestern United States, Anderegg *et al.* (2015) successfully
110 demonstrated a link between observed mortality of *Populus tremuloides* and a climatic water
111 deficit metric (the difference between potential and actual evapotranspiration), then inferred

112 widespread future mortality based on coupled climate model projections and their observed
113 mortality threshold. Where extensive monitoring networks exist (e.g. many countries in
114 Europe), tree mortality has been empirically linked to climate variability (anomalies in
115 temperature and precipitation) and tree age (Neumann *et al.*, 2017). In Australia, based on the
116 17 identified tree mortality events, Mitchell *et al.* (2014) used the intensity and duration of
117 drought, in combination with heatwaves to define a common probabilistic climatic threshold
118 for all vegetation types across Australia. They found that species in Australian ecosystems
119 were resilient to the majority of historic climatic conditions but are likely to experience
120 greater drought mortality risk by 2050. Such statistical approaches are powerful, but unless
121 underpinned by extensive mortality data sets (e.g. Neumann *et al.* (2017)), they lack the
122 sophistication to distinguish between regional, or even species behaviour (fundamentally
123 limited by the climate data resolution, which is typically coarse). These statistical approaches
124 also assume that the presentation of climate stresses that occurred in the past will be
125 replicated in the future (i.e. with no change in the interaction between soil moisture, vapour
126 pressure deficit (D), temperature and atmospheric carbon dioxide (Kelly *et al.*, 2016)) and that
127 there is no systematic acclimation and/or adaptation by the vegetation as the climate changes.

128 Thus, despite numerous field and manipulation experiments leading to advances in our
129 physiological understanding of the impact of drought, global-scale mortality thresholds
130 remain elusive (Choat *et al.*, 2012; Mencuccini *et al.*, 2015). In places where we do not yet
131 know the *in situ* mortality thresholds, we are unlikely to be able to link tree mortality to
132 climatic water deficit metrics or hydraulic traits alone, limiting our ability to forecast drought
133 impact globally. Consequently, we might opt for a more physiological approach that
134 integrates climatic stress through the soil-plant-atmosphere continuum via a model. However,
135 simulating the impact of water stress on vegetation function is a key weakness shared
136 amongst land surface schemes used in climate models (Galiano *et al.*, 2010; Egea *et al.*, 2011;

137 Powell *et al.*, 2013; De Kauwe *et al.*, 2015b; Christoffersen *et al.* 2016; Ukkola *et al.*, 2016a)
138 and very few approaches mechanistically link soil moisture stress and turnover of plant
139 tissues (but see Xu *et al.*, 2016), or directly simulate drought-induced mortality.

140 Our goal in this study was to examine whether we can use this physiological understanding of
141 drought mortality to make predictions at landscape scale. We embedded a representation of
142 plant hydraulics into the Australian land surface model, CABLE (Community Atmosphere–
143 Biosphere Land Exchange). We extend the model by incorporating the “second” drought
144 phase (after stomata have closed), allowing water to continue to be lost via cuticular
145 conductance (Choat *et al.*, 2018). We parameterised this new CABLE-Hydraulics based on a
146 drought manipulation experiment on 12 woody species originating from a broad precipitation
147 gradient (mean annual precipitation: 188–1125 mm yr⁻¹) across southeastern Australia (Li *et*
148 *al.*, 2018). We then applied the new model at the landscape scale to make predictions of
149 hydraulic failure due to drought in the Millennium (2000–2010) and “Big Dry” (2017–2019)
150 droughts. We used our model simulations to identify if, where and when, species were most
151 vulnerable to drought-induced mortality across South-East Australia (study area shown in
152 Figure S3).

153 **Methods**

154 *Model description*

155 CABLE is a land surface scheme, which can be run offline with prescribed meteorological
156 forcing (Wang *et al.*, 2011; De Kauwe *et al.*, 2015b; Ukkola *et al.*, 2016b; Decker *et al.*,
157 2017; Haverd *et al.*, 2018), or fully coupled (Pitman *et al.*, 2011; Lorenz *et al.*, 2014) within
158 the Australian Community Climate Earth System Simulator (ACCESS, see
159 <http://www.accessimulator.org.au>; Kowalczyk *et al.* (2013)).

160 CABLE simulates the carbon, energy and water fluxes at the land surface, representing the
161 vegetation using a single layer, two-leaf (sunlit/shaded) canopy model (Wang & Leuning,
162 1998), with a detailed treatment of within-canopy turbulence (Raupach, 1994; Raupach *et al.*,
163 1997). In the model, soil water and heat conduction are numerically integrated over six
164 discrete soil layers (4.6 m depth) following the Richards equation. The model groups
165 vegetation globally into 11 plant functional types (PFTs). CABLE has the capacity to be run
166 with an interactive biogeochemistry module (nitrogen and phosphorus) (Wang *et al.*, 2010)
167 and vegetation demography model (Haverd *et al.*, 2014), but both of these were switched off
168 for our simulations because leaf area index was prescribed (see below).

169 A complete description of the model can be found in Kowalczyk *et al.* (2006) and Wang *et al.*
170 (2011). The model source code can be accessed freely after registration at
171 <https://trac.nci.org.au/trac/cable>. In this paper we used CABLE revision 6134.

172 *Simulating hydraulic failure*

173 Following Xu *et al.* (2016), we introduced an augmented plant hydraulic module (“Desica”)
174 into CABLE to replace the default empirical representation of drought stress based on
175 volumetric soil moisture content, weighted by the fraction of roots in each of CABLE’s six
176 soil layers (De Kauwe *et al.*, 2015b). Desica tracks water flow through the soil-plant-
177 atmosphere continuum based on the gradient in water potentials between the leaf (Ψ_l , MPa),
178 stem (Ψ_x , MPa) and the weighted average of the soil (Ψ_{sw} , MPa).

179 For each soil layer (i), we related the volumetric water content (θ , $\text{m}^3 \text{m}^{-3}$) to soil water
180 potential (Ψ_s , MPa) following Campbell (1974):

$$181 \quad \Psi_{s,i} = \Psi_e \left(\frac{\theta}{\theta_{sat}} \right)^{-b} \quad (1)$$

182 where Ψ_e (MPa) is the air entry point water potential, θ_{sat} ($\text{m}^3 \text{m}^{-3}$) is the soil volumetric
 183 moisture content at saturation and b (unitless) is the empirical pore size distribution index
 184 which approximates the slope of the soil-water retention curve (Clapp & Hornberger, 1978).

185 To obtain a representative value of whole root-zone Ψ_s , we weighted the average Ψ_s for each
 186 of the six soil layers by the weighted soil-to-root resistance to water uptake (R_s , $\text{MPa s m}^2 \text{m}^{-3}$)
 187 of each layer (Williams *et al.*, 2001a; De Kauwe *et al.*, 2015b). Following Gardner (1960),
 188 for each soil layer, R_s is defined as:

$$189 \quad R_{s,i} = \frac{\ln\left(\frac{r_s}{r_r}\right)}{2\pi l_r D K_{soil}} \quad (2)$$

190 where r_s is the mean distance between roots (m) (Williams *et al.* 2001a), r_r is the fine root
 191 radius (m) (Williams *et al.* 2001a), D is the depth of the soil layer (m) (Jackson *et al.* 1996), l_r
 192 is the fine root density (m m^{-3}) (Williams *et al.* 2001a) and K_{soil} is the soil hydraulic
 193 conductivity ($\text{m}^2 \text{s}^{-1} \text{MPa}^{-1}$) which depends on soil texture and soil water content. The total
 194 below-ground soil-to-root resistance is calculated as the reciprocal of the summed inverses of
 195 each soil layer's resistance.

196 To solve the leaf (Ψ_l) and stem water potentials Ψ_x requires integration, which can lead to an
 197 instability due to the dependence on Ψ_l . Xu *et al.* (2016) proposed a simplification by treating
 198 Ψ_x as a constant ($\Psi_{x_{t-1}}$) by using the previous time step (Equation 5), which allows Ψ_l to be
 199 solved analytically. Similarly, the soil water potential is assumed to be a constant ($\Psi_{sw_{t-1}}$)

200 when calculating Ψ_x (Equation 8). Xu *et al.* (2016) argued that their simplifications did not
 201 result in large biases at the 10-minute timescale. Here, we followed their approach at the 30-
 202 minute timescale due to the limitations of the forcing data.

203 Ψ_l is solved as:

$$204 \quad \Psi_l = \frac{(a_l \Psi_{l_{t-1}} + b_l) e^{(a_l \Delta t)} - b_l}{a_l} \quad (3)$$

205 where $\Psi_{l_{t-1}}$ is the leaf water potential from the previous time step (MPa), Δt is the timestep
 206 (30 minutes in this case), a_l and b_l are solved as:

$$207 \quad a_l = \frac{-k_{xl}}{C_l} \quad (4)$$

$$208 \quad b_l = \frac{\Psi_{x_{t-1}} k_{xl} - (\text{LAI} \cdot E)}{C_l} \quad (5)$$

209 where k_{xl} is the conductance from the stem water store to the leaves ($\text{mmol m}^{-2} \text{s}^{-1} \text{MPa}^{-1}$), E
 210 is the transpiration flux from the canopy ($\text{mmol m}^{-2} \text{s}^{-1}$), C_l the leaf capacitance ($\text{mmol m}^{-2} \text{s}^{-1}$
 211 MPa^{-1}) scaled up by the canopy leaf area (LAI, $\text{m}^2 \text{m}^{-2}$).

212 Ψ_x is then calculated as:

$$213 \quad \Psi_x = \frac{(a_x \Psi_{x_{t-1}} + b_x) e^{(a_x \Delta t)} - b_x}{a_x} \quad (6)$$

214 where $\Psi_{x_{t-1}}$ is the stem water potential from the previous time step. a_x and b_x are solved as:

$$215 \quad a_x = \frac{-k_{sx}}{C_s} \quad (7)$$

$$216 \quad b_x = \frac{\Psi_{sw_{t-1}}k_{sx} - J_{sl}}{C_s} \quad (8)$$

217 where $\Psi_{sw_{t-1}}$ is the weighted soil water potential from the previous timestep. k_{sx} is the
 218 conductance from the soil to the stem water store ($\text{mmol m}^{-2} \text{s}^{-1} \text{MPa}^{-1}$), which includes the
 219 weighted soil-to-root conductance to water uptake (i.e. $1 / R_s$) and the conductance from the
 220 root surface to the stem water pool (assumed to be halfway between the roots and the leaves).
 221 C_s is stem capacitance ($\text{mmol m}^{-2} \text{s}^{-1} \text{MPa}^{-1}$) scaled up by the leaf area-to-sapwood area ratio
 222 (LA:SA), sapwood density (kg m^{-3}) and height (m). J_{sl} is the flux of water from the stem to
 223 the leaves ($\text{mmol m}^{-2} \text{s}^{-1}$), calculated as:

$$224 \quad J_{sl} = \frac{(\Psi_l - \Psi_{l_{t-1}})C_l}{\Delta t} + (\text{LAI} \cdot E) \quad (9)$$

225 Xu *et al.* (2016) iteratively solved an optimal stomatal conductance model based on Ψ_l .
 226 Instead, we used a stomatal conductance model that assumes a sigmoidal sensitivity to Ψ_l
 227 (Tuzet *et al.*, 2003):

$$228 \quad g_s = \max(g_{min}, 1.6g_1 \frac{A_n}{C_s} f(\Psi_l)) \quad (10)$$

229 where g_s ($\text{mol m}^{-2} \text{s}^{-1}$) is the stomatal conductance to water vapour, g_{min} is the water lost via
 230 cuticular conductance from internal stored water (Choat *et al.*, 2018; Blackman *et al.*, 2019),
 231 A_n is the net assimilation rate ($\mu\text{mol m}^{-2} \text{s}^{-1}$), C_s is the CO_2 concentration at the leaf surface ($\mu\text{mol mol}^{-1}$) and g_1 (unitless) is a fitted constant representing the slope of the sensitivity of g_s

233 to A_n (-). The factor of 1.6 converts from conductance to CO₂ to conductance to water vapour.

234 $f(\Psi_l)$ is a sigmoidal function defined as:

$$235 \quad f(\Psi_l) = \frac{1 + e^{(S_f \Psi_f)}}{1 + e^{(S_f(\Psi_f - \Psi_l))}} \quad (11)$$

236 where S_f (MPa⁻¹) determines the shape of the response of g_s to Ψ_l and Ψ_f (MPa) is a

237 reference water potential.

238 Xylem conductance (k_x) was assumed to decline via cavitation: *i.e.* a relative drop from a

239 maximum value (the maximum plant hydraulic conductance, k_{plant} ; mmol m⁻² leaf s⁻¹ MPa⁻¹)

240 following a Weibull model as Ψ_x declines (Ogle, 2009):

$$241 \quad \frac{k_x}{k_{plant}} = \left(\frac{100 - 50^p}{100} \right) \quad (12)$$

242
243
244

242 where

$$243 \quad p = \left(\frac{\Psi_x}{|P_{50}|} \right)^{\frac{|P_{50}| S_{50}}{V}} \quad (13)$$

244 and

$$245 \quad V = (50 - 100) \ln(1 - 50/100) \quad (14)$$

246 where P_{50} is xylem pressure inducing 50% loss of hydraulic conductivity due to embolism

247 (MPa) and S_{50} (% MPa⁻¹) is the slope of the percentage loss of hydraulic conductivity (PLC)

248 at P_{50} .

249 We assume that cavitation can be fully recovered following rainfall (Xu *et al.*, 2016). We
250 extend Xu *et al.* (2016) by allowing CABLE to track hydraulic failure until it reaches the
251 critical threshold of hydraulic failure associated with mortality. To achieve this, we assume
252 that following stomatal closure, Ψ_x continues to decrease as water is lost via g_{\min} (Choat *et al.*,
253 2018; Blackman *et al.*, 2019). Previous work has shown a strong link between a threshold
254 corresponding to an 88% loss of stem hydraulic conductance (P_{88}) and drought mortality (Urli
255 *et al.*, 2013; Li *et al.*, 2015, 2018). Here, we do not equate P_{88} with mortality, but rather
256 interpret it as indicative of the vegetation approaching a point of hydraulic stress likely to
257 correspond to mortality, Ψ_{crit} . We make this distinction because each grid cell ($\sim 5 \text{ km}^2$) would
258 contain a number of trees, not all of which would be dead. To bridge the gap from Ψ_{crit} to
259 mortality would require stochastic approaches that are beyond the scope of the study.

260 *Model simulations*

261 *New land-cover map*

262 We replaced the standard vegetation land-cover map used in CABLE with a five-class land-
263 cover map (Figure S4) derived from the National Vegetation Information System (NVIS,
264 [https://www.environment.gov.au/land/native-vegetation/national-vegetation-information-](https://www.environment.gov.au/land/native-vegetation/national-vegetation-information-system)
265 [system](https://www.environment.gov.au/land/native-vegetation/national-vegetation-information-system)). NVIS classifies the extent and distribution of vegetation types in Australian
266 landscapes into 32 classes. We reclassified the vegetation classes that make up South-East
267 Australia based on the drought manipulation experiments on 12 dominant tree species, so as
268 to represent five major woody vegetation types
269 (<https://data.nsw.gov.au/data/dataset/4b6f1b3f-f33a-4e56-a6dd-5b052f28a361>) in New South
270 Wales, Australia (see below). Our five new vegetation classes (Figure S4) were: (i) rainforest
271 (RF); (ii) wet sclerophyll forest (WSF); (iii) dry sclerophyll forest (DSF); (iv) grass woodland
272 (GRW); and (v) semiarid woodland (SAW).

273 *Model parameterisation*

274 Each of the five new vegetation classes was parameterised based on the hydraulic and
275 physiological traits measured in the drought manipulation experiments conducted by Li *et al.*
276 (2018), Li *et al.* (2019) and Blackman *et al.* (2019). Full details are given by Li *et al.* (2018)
277 but in brief, after 4 months of growth, seedlings of each species were transplanted to a
278 polytunnel growth facility at Western Sydney University. Seedlings were placed into 25 l
279 bags filled with native loamy sand top-soil. There were two drought phases: (i) plants were
280 first dried until the point of visual wilting and then re-watered for 10 days to allow for full
281 recovery; and then (ii) water was completely withheld to allow plants to use up all of their
282 available water reserves. A full suite of hydraulic and physiological traits was measured
283 during the second dry-down period.

284 Hydraulic traits measured on young plants grown under common conditions are assumed to
285 reflect trait values of mature trees growing in the field. In the case of stem xylem cavitation
286 resistance, there is evidence that this is true for *Eucalyptus* species, with P_{50} measured on the
287 main stem axis of younger plants closely matching P_{50} of branches collected from mature
288 trees in the field (Bourne *et al.*, 2017; Blackman *et al.*, 2019). Stem P_{50} also appears to have
289 limited plasticity in response to growth environment (Lamy *et al.*, 2014). Leaf hydraulic
290 traits may be expected to vary more in response to growth environment and this variation
291 could lead to bias in model output.

292 Species traits were averaged within vegetation classes as grouped by Li *et al.* (2018).

293 Specifically for each vegetation class, we estimated values for P_{50} , k_{plant} (plant hydraulic
294 conductance, $\text{mmol m}^{-2} \text{ leaf s}^{-1} \text{ MPa}^{-1}$), C_i , C_s , V_{cmax} (maximum carboxylation rate at 25 °C, μ
295 $\text{mol m}^{-2} \text{ s}^{-1}$), J_{max} (maximum rate of electron transport at 25 °C, $\mu\text{mol m}^{-2} \text{ s}^{-1}$), g_1 ; g_{min} (mmol

296 $\text{m}^{-2} \text{s}^{-1}$), S_{50} , S_f (MPa^{-1} , assumed to be fixed) and Ψ_f . The key parameter values are shown in
297 Table 1.

298 To apply the model at the landscape scale we had to make several simplifying assumptions.
299 To scale up the measured branch capacitance and obtain an estimate of total C_s , we used
300 experimentally measured estimates of LA:SA and sapwood density (Table 1) and height
301 estimates from LiDAR data (Simard *et al.*, 2011). We estimated heights of 32 m, 29 m, 25 m,
302 11 m and 7 m for the RF, WSF, DSF, GRW and SAW vegetation classes based on the median
303 heights of pixels within each vegetation class derived from the Geoscience Laser Altimeter
304 System, LiDAR data (Simard *et al.*, 2011). Root biomass was prescribed based on the
305 measured fine root biomass at the Eucalyptus woodland Free Air CO_2 Enrichment research
306 facility in native Australian forest experiment – 832 g C m^{-2} (Jiang *et al.*, 2020) – and used to
307 calculate l_r in Equation 2. This biomass value is comparable to values used in previous
308 studies (Williams *et al.*, 2001b; Schwarz *et al.*, 2004; Fisher *et al.*, 2007; Hill *et al.*, 2011) but,
309 in reality, root biomass would vary spatially. We found that our single site model results were
310 insensitive to varying fine root biomass between 200 and 1000 g C m^{-2} (Transpiration Root
311 Mean Squared Error, $\text{RMSE} < 1 \text{ W m}^{-2}$). Root density (0.5 g cm^{-3}) and root resistivity (25
312 MPa s g mmol^{-1}) were prescribed following Williams *et al.* (2001b) and Bonan *et al.* (2014),
313 respectively. Bonan *et al.* (2014) found their plant hydraulics model to be most sensitive to
314 root resistivity among the root parameters. CABLE-hydraulics, however, showed no notable
315 sensitivity to root resistivity (Transpiration Root Mean Squared Error, $\text{RMSE} < 1 \text{ W m}^{-2}$),
316 even when assuming a value as high as $150 \text{ MPa s g mmol}^{-1}$.

317 In our model simulations, we also assumed that each 5 km^2 grid cell was only occupied by
318 trees with a leaf area prescribed based on satellite data. This assumption is unrealistic
319 (because a large proportion of South-East Australia is composed of a mixture of trees,

320 agricultural land and grasslands); we made it because we aimed to explore drought-induced
321 tree mortality. As models (even dynamic vegetation models) do not realistically account for
322 below-ground water competition (see Fisher et al. 2018 for a review of the state-of-the-art),
323 our assumption is the same as running a tiled model (grid box divided into fractions of
324 different surface type) and simply analysing the tree fraction. The model results are
325 interpreted accordingly.

326 *Model forcing*

327 We performed offline simulations for South-East Australia (~400,000 km²) using gridded, 30-
328 minute meteorological forcing of precipitation, downward shortwave and longwave radiation,
329 surface air temperature, surface specific humidity, surface wind speed, surface air pressure
330 and atmospheric carbon dioxide concentration. We ran the model over the period 2000–2010
331 (Millennium Drought; spin-up 1995–1999) and 2017–2019 (Big Dry; spin-up 2011–2016) at
332 a resolution of 0.05° (~5 km²). The meteorological data were sourced from the Bureau of
333 Meteorology’s Australian Water Availability Project (AWAP) (Jones *et al.*, 2009) and the
334 near-surface wind data of McVicar *et al.* (2008; McVicar, 2011). Data were downscaled from
335 daily inputs to 3-hourly time steps using a weather generator (Haverd *et al.*, 2013) and then
336 linearly interpolated to obtain 30-minute forcing. For the precipitation forcing, 30-minute data
337 were obtained by first translating the 3-hourly rate to 30-minutes time slots and then assuming
338 zero rainfall for the additional 30-minutes time slots. Wind data from McVicar (2011) were
339 not available for 2019 so a monthly climatology from 2014–2018 was substituted.

340 CABLE was run with prescribed LAI based on a climatology (1999–2017) derived from the
341 Copernicus LAI product, which is distributed by the Copernicus Global Land portal
342 (<http://land.copernicus.eu/global/>). The Copernicus LAI product is derived from

343 SPOT/VEGETATION and PROBA-V data at 10-day intervals at a 0.01° (~1 km) spatial
344 resolution using a neural network approach. To force CABLE, we degraded the data from a
345 resolution of 0.01° to 0.05° . By prescribing LAI we avoid the need for a long model spin-up,
346 only requiring five years to stabilise the soil temperature and root-zone soil moisture.
347 Prescribing the LAI also avoids the assumption that the forest is in equilibrium with the
348 current climate, as would be the case had we spun up the model's carbon cycle. The model
349 was therefore spun up using five-year periods (repeating the meteorological forcing, 1995-
350 1999 and 2011-2016, see below).

351 Soil properties (e.g. texture, soil hydraulic and thermal characteristics) for CABLE were
352 based on the SoilGrids (Hengl *et al.*, 2017) data. Data were degraded using local area
353 averaging from 250m to 0.05° for simulations. We also tested the sensitivity of our results to
354 the 90m Soil and Landscape Grid of Australia soil dataset
355 (<https://www.clw.csiro.au/aclep/soilandlandscapegrid>) degraded to 0.05° (~5 km) but found
356 no significant impact arising from the choice of dataset. As is standard in CABLE, we
357 assumed vertically uniform soil texture based on the weighted average of the 2 m SoilGrids
358 data.

359 *Sensitivity experiment*

360 To better understand the resilience to drought conferred by hydraulic traits, we also carried
361 out a model sensitivity experiment. Starting from a wet soil profile and without further
362 precipitation, we asked: how long would it take for each vegetation class to reach Ψ_{crit}
363 (assumed to be P_{88})? For each of the five vegetation types, we sampled (5 samples) $\pm 35\%$ of
364 the measured trait averages for g_{min} , P_{50} , C_1 and C_s . We also sampled between the interquartile
365 range (i.e. difference between 75th and 25th percentiles) LAI value, θ_{sat} and b found within

366 the geographical range of each vegetation class. Temperature was fixed to 35°C and a relative
367 humidity set to 10%. A temperature of 35°C is common in summers in South East Australia:
368 in New South Wales, the average maximum temperature during summer is 31°C and the 10
369 hottest summers on record all have days exceeding 40°C (Bureau of Meteorology;
370 <http://www.bom.gov.au/>).

371 For computational efficiency, we coupled the plant hydraulics module (Desica) to a big-leaf
372 canopy module (with the same coupled photosynthesis-stomatal conductance approach from
373 CABLE) and a single soil water “bucket” (of varying depth between 0.1 and 1 m), where the
374 only losses from the soil profile were assumed to be due to transpiration ($E=1.6g_sD$). In total,
375 we ran 140,625 simulations in the sensitivity experiment.

376 The sensitivity experiments were designed to examine the vegetations’ tolerance to extreme
377 drought conditions but as the simulations use an imposed extreme climate and a simpler
378 representation of soil hydrology, the exact simulated day of Ψ_{crit} should be interpreted
379 cautiously. Instead, we were interested in the relative simulated differences between to Ψ_{crit}
380 for the vegetation classes.

381 *Data sets used*

382 *Satellite data*

383 To test whether our model realistically predicts where water stress occurred during the
384 Millennium Drought, we calculated anomaly maps (percent difference) using remote sensing
385 estimates of vegetation optical depth (VOD) and normalised difference vegetation index
386 (NDVI).

387 VOD data describes the attenuation of microwave wavelengths through the vegetation layer
388 and has been assumed to be most sensitive to above-ground vegetation water content and
389 changes in leaf/branch biomass (van Dijk *et al.*, 2013). We used two VOD datasets to
390 quantify the change in the vegetation due to drought. For the Millennium drought, we
391 calculated the average and greatest difference from a baseline average between 1993 and
392 1999, using a merged passive microwave VOD product (Liu *et al.*, 2011). For the Big Dry
393 (2017-2018) we estimated an anomaly from a baseline between 2010 and 2016. In the latter
394 case, we used the land parameter data record (LPDR) version 2 VOD product (Du *et al.*,
395 2017), which uses retrievals from the Advanced Microwave Scanning Radiometer for EOS
396 (AMSR-E) and the Advanced Microwave Scanning Radiometer 2 (AMSR2). We used two
397 different products because no single microwave sensor covers the entire period.

398 NDVI quantifies the photosynthetically active radiation that is absorbed by vegetation and so
399 captures changes in foliar vegetation during periods of water stress. For the Millennium
400 drought, we calculated the average and greatest difference from a baseline average between
401 1993 and 1999 (baseline chosen to match VOD). For the Big Dry (2017-2018), we estimated
402 an anomaly from a baseline between 2010 and 2016. In each case, we used the NOAA
403 Climate Data Record version 4 product based on the Advanced Very High Resolution
404 Radiometer (AVHRR) sensor (Vermote, 2019).

405 In both remotely sensed estimates, we excluded the final summer period from our anomaly
406 calculation for the Big Dry (2019), owing to the potential contamination due to fires in South-
407 East Australia.

408 *Climatic water deficit*

409 A number of approaches have been used in the literature to quantify drought impact via a
410 climatic water deficit. To explore the usefulness of these approaches, we calculated an
411 estimate of climatic water deficit: precipitation minus potential evapotranspiration (P-PET).
412 For the calculation of mean P-PET at 0.05° resolution, precipitation data was taken from
413 AWAP and PET was calculated following Priestley & Taylor (1972) from AWAP monthly
414 incoming shortwave radiation (converted to sunshine hours) and mean air temperature using
415 the R package rstash (https://github.com/rhyswhitley/r_stash; Davis *et al.* (2017)).

416 *Ozflux eddy covariance*

417 To evaluate the new hydraulics module, we ran CABLE-Hydraulics at two woodland sites
418 within the Australian eddy covariance network: the Wombat state forest (37.42°S, 144.09°E;
419 Griebel *et al.* (2016)) and Tumbarumba (35.65°S, 148.15°E; Keith *et al.* (2012)) sites. We
420 assumed that the Wombat site could be represented as a DSF and Tumbarumba as a WSF
421 vegetation type. Those sites were chosen because the measurements records cover periods
422 with significant drought. The CABLE outputs compared to half-hourly eddy covariance
423 measurements of the exchange of carbon dioxide, energy, and water vapour obtained from
424 OzFlux (<http://www.ozflux.org.au/>, last access: 26 April 2017). We used Level 6 gap-filled
425 data following Isaac *et al.* (2017). Flux data were pre-processed using the FluxnetLSM R
426 package Ukkola *et al.* (2017) and then screened to retain measured and good-quality gap-
427 filled data.

428 *Analysis code*

429 All analysis code is freely available from
430 https://github.com/mdekauwe/SE_AUS_drought_risk_paper.git

431 Results

432 *Sensitivity experiment*

433 Figure 1 shows the time taken for each vegetation class to reach Ψ_{crit} , expressed as a
434 histogram. Varying all the possible trait combinations leads to a marked overlap in
435 distributions of the simulated day of Ψ_{crit} , with the exception of the SAW class. Despite this
436 overlap, there is a notable separation in the peaks of the WSF and RF classes and the GRW
437 class has a very broad upper tail, which overlaps with the SAW class. Our model results
438 suggest that the WSF class was the most vulnerable and the least vulnerable was SAW.
439 Perhaps counter-intuitively, the RF class emerges as more resilient than all classes except
440 SAW (but note broad upper tail of GRW). This result is due to a combination of the very
441 negative P_{50} (Table 1), which is the third most resistant among the five vegetation classes and
442 the lowest g_{min} value, meaning that the rate of cuticular water loss is relatively low. Overall,
443 g_{min} , LAI and P_{50} (in that order of importance) were the predictors that contributed most to
444 vegetation resilience (assessed using partial residual plots; not shown). Finally, the
445 overlapping distributions in the simulated day of Ψ_{crit} , imply that when embedded within
446 CABLE, our model should predict gradients in Ψ_{crit} rather than sharp boundaries that follow
447 vegetation class boundaries.

448 *Drought simulation at eddy-flux sites*

449 Figures 2 and 3 show two flux site-scale comparisons between observations of latent heat flux
450 (LE), flux-derived gross primary productivity (GPP) and simulated fluxes by standard
451 CABLE (Control) and the new CABLE-Hydraulics (Hydraulics) model. At both sites there is

452 evidence of pronounced water stress (shown by the gaps between rainfall events). These site-
453 scale simulations allow us to evaluate the new hydraulics model.

454 Introducing a representation of plant hydraulics leads to marked improvements in CABLE's
455 capacity to simulate carbon and water fluxes during periods of water stress. During the
456 periods of water stress, the hydraulics model approximately halves the error in the modelled
457 LE relative to the Control, whilst also improving the simulation of GPP. At Wombat (Figure
458 2), the RMSE in LE was reduced from 37 W m^{-2} to 20 W m^{-2} (Pearson's correlation
459 coefficient, r : 0.61 vs 0.82) and at Tumbarumba (Figure 3), the RMSE was reduced from 56
460 W m^{-2} to 36 W m^{-2} (r : 0.31 vs 0.58). These improvements result from the replacement of the
461 empirical drought-stress function based on soil texture (Fig S5; Figures S6 and S7 show the
462 evolution of modelled water potentials at both sites) with two drought-stress modifiers based
463 on Ψ_1 , Ψ_x and measured hydraulic traits (e.g. P_{50}). Whilst it is clear that the new hydraulics
464 could be improved further (i.e. the sensitivity in both the control and hydraulics model
465 relative to the control remains similar), it is important to note that these simulations have not
466 been tuned to any of the sites.

467 *Climatic water deficit*

468 Figure 4 shows the widely used climatic water deficit metric ($P-PET$) prior to (panel a) and
469 the difference (during the Millennium Drought minus prior, panel b). In an environment
470 where PET is always high (due to high solar radiation and temperature), this approach is of
471 limited value for inferring drought impact on the vegetation, as panel b show little
472 distinguishable difference (hence we do not show the Big Dry). These climatic deficit maps
473 (Figure 4) can be compared to the year-to-year rainfall decile maps, which show distinct
474 spatial patterns (Figure S1).

475 Contrasting these P–PET deficit maps with maps that depend on actual evapotranspiration
476 (AET), as simulated via CABLE-Hydraulics during the Millennium drought (Figure 5a) and
477 the Big Dry (Figure 5b), clearly highlights the spatially heterogeneous impact of the drought.
478 Both maps show greater deficit inland (moving west), although the regions of greatest deficit
479 differ in spatial location and magnitude between the droughts. Overall, the simulated water
480 stress (lower P–AET) was noticeably greater throughout South-East Australia during the Big
481 Dry compared to the Millennium Drought, particularly east of 145°E.

482 *Simulated hydraulic failure*

483 In the coastal regions, despite the simulated (P–AET) deficit due to the drought (cf. Figures 5a
484 to 5b focussing on north of 32°S and south of 37°S), CABLE simulates no signs of
485 approaching Ψ_{crit} (the xylem pressure inducing 88 % loss of hydraulic conductivity) at any
486 point during either drought (Figures 6a,b). These predictions are consistent with the satellite
487 anomaly maps (VOD and NDVI), which both suggest limited impact along the coast of
488 South-East Australia (Average anomaly: Figures 7 and 8; Greatest anomaly: Figures S8 and
489 S9). Moving west and inland, the impact of the Big Dry is more marked than that of the
490 Millennium drought, with many regions approaching a greater maximum PLC ~40–50 %
491 (145°E to 151°E). In both droughts, CABLE consistently simulates large areas that reach Ψ_{crit}
492 (north of 35°S and west of 145°E). In those regions, CABLE-Hydraulics indicates that trees
493 would be unlikely to survive those two most recent droughts. Figure S10 shows the
494 timecourse of Ψ_{sw} , Ψ_{l} and Ψ_{x} for four representative pixels from the GRW and SAW
495 vegetation classes during the Big Dry. As can be seen by comparing Figures S10c and S10d,
496 greater LAI (Figure S10d, see also sensitivity experiment) and so higher losses via g_{min} leads
497 to increased water stress for SAW pixels.

498 Comparing the regions of greatest drought impact according to the remote sensing data
499 (Average anomaly: Figures 7 and 8; Greatest anomaly: Figures S8 and S9) to the maps of
500 maximum PLC (Figure 6), there is a reasonable degree of spatial agreement. The regions of
501 greatest drought impact in both the VOD and NDVI maps are also areas of significant (>50
502 %) PLC. The higher agreement between the PLC map and the NDVI data, may relate to our
503 assumption of perfect recovery upon rewatering (see discussion). The NDVI data for the Big
504 Dry (Figure 8b) shows a more marked decline in green canopy cover than the Millennium
505 drought (Figure 8a) and this is broadly consistent with the PLC maps (Figure 6). CABLE
506 does appear to miss the decline in NDVI south of 37°S; however, this feature is not evident in
507 the VOD data (Figure 7b). Overall, CABLE simulates a more widespread impact due to
508 drought than the satellite data but is qualitatively consistent in identifying the regions of
509 greatest impact. It is worth noting that CABLE is simulating uniform tree cover throughout
510 the domain, so the evaluation against the satellite data is only indicative of potential drought
511 impact.

512 Figure 9 shows the PLC map as an average timeseries for each tree class, allowing us to
513 visualise the point during the droughts at which CABLE simulated the greatest impact. In the
514 Millennium Drought (Figure 9a), the impact was greatest for all vegetation classes during mid
515 2002 – mid 2003 and mid 2006 – mid 2007, which is consistent with the rainfall decile maps
516 (Figure S1). There is an increasing accumulated level of drought impact (GRW and SAW) as
517 illustrated by a year-on-year increase in PLC between 2003 and 2007 (Figure 9). For the Big
518 Dry, Figure 9b, there is a worsening state of the vegetated land surface leading into the 2019–
519 2020 austral spring/summer.

520 *Sensitivity to soil moisture*

521 PLC increases as soil water declines for the Millennium drought (Figure 10; Figure S11
522 shows the Big Dry). We can see that in both droughts the DSF, GRW and SAW classes had
523 very low available soil moisture in their top four layers ($\theta < 0.17 \text{ m}^3 \text{ m}^{-3}$). For the DSF class
524 this led to little increase in PLC, but by contrast the simulated PLC for the GRW exceeded
525 20% for a large number of pixels. Given the similarity in the parameterised traits (Table 1, see
526 also Figure 1), these differences show the additional stress imposed by the climate, *e.g.*
527 through temperature and vapour pressure deficit. This sensitivity to climate becomes more
528 pronounced at low volumetric soil water content values (cf. GRW and SAW) when the total
529 below-ground soil-to-root resistance (see Equation 2) is greatest and the Ψ_x and Ψ_l drop
530 significantly diurnally, leading to higher PLC values. In our sensitivity experiment (Figure 1),
531 we sampled the interquartile range of LAI found within the SAW vegetation class and
532 matching expectations based on traits (Table 1), the SAW appeared more resilient than other
533 classes. However, for a ~ 1 % of pixels within the SAW vegetation class, LAI values exceeded
534 $1.5 \text{ m}^2 \text{ m}^{-2}$, which is likely to reflect non-tree contributions (cf. Figures S10c and S10d).

535 Discussion

536 *Did trees die during the droughts?*

537 Globally, Australia stands out with limited reports of recent widespread drought-induced tree
538 mortality (Allen *et al.*, 2015). There are a number of studies that have historically documented
539 drought-related tree mortality across Australia (Hopkins, 1973; Landsberg, 1985; Pook, 1986;
540 Fensham *et al.*, 2009; Ross & Brack, 2015), but reports of mortality during the decadal
541 Millennium Drought are surprisingly few (Keith *et al.*, 2012). This contrasts with recent
542 droughts in the California and Texas, in which severe droughts were estimated to have killed
543 100 million and 300 million trees, respectively (Asner *et al.*, 2016; Moore *et al.*, 2016;

544 Service, 2016). Were tree deaths during the Millennium Drought simply not recorded? Or
545 instead are Australian tree species exceptionally resilient to drought and did not approach
546 critical hydraulic thresholds? For large areas of South-East Australia (that supports a large
547 proportion of Australia's forests), CABLE-Hydraulics did not predict that the trees
548 approached Ψ_{crit} in either drought (Figure 6). These results were qualitatively in spatial
549 agreement with remote sensing estimates, noting that the remote sensing estimates do not
550 show mortality (Average anomaly: Figures 7 and 8; Greatest anomaly: Figures S8 and S9).
551 However, the model is likely to be too sensitive to water stress in the initial phase (stomatal
552 closure) of drought response (Figures 2 and 3), and too insensitive in the second phase
553 (cuticular water loss), where we do not have data to evaluate the model.

554 Our model did predict potential drought-induced mortality across the extremely arid regions
555 in northwestern New South Wales (Fig. S3), but this result should be interpreted cautiously.
556 To explore tree-related drought mortality, we assumed that trees were able to grow all across
557 South-East Australia. In the northwestern region we are approaching the Simpson desert
558 where Donohue *et al.* (2009) used a satellite-derived estimate of persistent tree cover (a proxy
559 for where trees grow) for this region to indicate that no trees grow there. However, trees
560 having the mallee growth form, characterised by multiple stems and a massive lignotuber, are
561 present, but are patchily located and sometimes in close proximity to river features. It has
562 been suggested that these mallee communities could be classified either as woodlands or as
563 shrublands given their physiognomy, which appears to be uniquely Australian (Whittaker *et*
564 *al.*, 1979). Thus, an alternative view of CABLE's prediction is that trees, as defined by the
565 five simulated habitat types, *should* not be able to live there during a drought without
566 additional water sources (e.g. groundwater).

567 Anecdotal and visual point-scale reports (e.g. the citizen science Dead Tree Detective project;
568 <https://biocollect.ala.org.au/acsa/project/index/77285a13-e231-49e8-b212-660c66c74bac>)
569 suggest extensive tree mortality during the Big Dry across South-East Australia. Much of this
570 mortality was observed during significant heatwaves in summer 2019, a period that we were
571 unable to examine in the remotely-sensed data owing to the extensive bushfires. These
572 observations would appear to be odds with our model predictions for the Big Dry (Figure 6b).
573 Our model simulations simulated broadly similar results between the two droughts we
574 examined, where the emerging reports point to a greater impact from the shorter, more-
575 intense Big Dry. This may imply that while we have improved simulation performance during
576 the initial phase of drought response by incorporating hydraulic function, more data are
577 needed to better constrain the second phase (see below). In situ measurements of leaf water
578 potential, carbohydrates reserves, leaf shedding, vulnerability to cavitation (Ψ_{50} , Ψ_{88}) and
579 capacitance, would be particularly valuable. In addition, the anecdotal observations of canopy
580 death during the heatwaves indicate that we need to more closely examine interactions
581 between drought and heatwaves (so-called compound events) and simulated vegetation
582 function in future work.

583 Emerging reports of canopy death are yet to be verified: many eucalypts may appear dead due
584 to total canopy defoliation following hydraulic failure *i.e.* they hit Ψ_{crit} and, yet the trees may
585 not be dead, since many eucalypts, resprout following rain (Nolan *et al.*, 2014). Furthermore,
586 trees may not die directly from drought, but due to many other factors that may be associated
587 with drought (e.g. pests and pathogens) (Weed *et al.*, 2013). Thus, attempts to predict drought
588 mortality may need to consider resprouting capacity as well as hydraulic failure.

589 Australian trees are likely to be among the first ecosystems to be exposed to extremes of
590 climate (e.g. higher temperatures) under climate change and insight into ecosystem responses

591 to extremes may be disproportionately valuable (van der Horst *et al.*, 2019) to developing
592 theory for trees world-wide. Most studies that have explored responses to drought compare
593 measured hydraulic traits but ignore differences in local climate. Or put another way, studies
594 have evaluated vulnerability simply from the axis of sensitivity and not accounted for risk too.
595 Our results highlight the importance of integrating both traits and climate to gain insight into
596 mortality predictions across species. In our (experimentally constrained) model simulations,
597 the divergence in ecosystem flux trajectories towards Ψ_{crit} is greater within vegetation classes
598 than what the traits themselves would imply (cf. PLC map, Fig. 6 and Table 1).

599 *Hydraulics models in land surface models*

600 Poor model performance during periods of water stress (Powell *et al.*, 2013; Medlyn *et al.*,
601 2016; Ukkola *et al.*, 2016a) have led authors to argue that we require a more mechanistic
602 approach to determine the impact of water stress on vegetation function in models (Sperry &
603 Tyree, 1988; McDowell *et al.*, 2013; Zhou *et al.*, 2013; De Kauwe *et al.*, 2015a; Sperry *et al.*,
604 2017). It is plausible that model improvements could be achieved by replacing the widespread
605 empirical functions based on soil moisture availability and texture with more mechanistic
606 representations of plant hydraulics. A series of land surface schemes have successfully
607 demonstrated this point with recent model advancements (Bonan *et al.*, 2014; Christoffersen
608 *et al.*, 2016; Xu *et al.*, 2016; Kennedy *et al.*, 2019; Eller *et al.*, 2020; Sabot *et al.*, 2020).
609 However, to date, the focus has predominantly been on individual sites (but see Xu *et al.*,
610 2016) and integrating trait measurements into viable global parameterisations for land surface
611 models remains a key challenge (not least due to the lack of high spatiotemporal resolution
612 climate data). Current coupled climate models do not adequately represent legacy effects of
613 drought (e.g. turnover of plant tissues, instantaneous recovery, etc), including drought-
614 induced mortality. Recovery after drought is not likely to be instantaneous (Saatchi *et al.*,

615 2013; Wigneron *et al.*, 2020), as commonly assumed by models, implying that surface energy
616 partitioning feedback on atmospheric processes may be in gross error, which may be
617 particularly important in future projections.

618 In this study, we introduced a hydraulics model into the CABLE LSM and made landscape-
619 scale (~400,000 km²) predictions of drought-induced mortality (Ψ_{crit}) during the Millennium
620 drought and Big Dry across South-East Australia. The new hydraulics model notably
621 improved simulations of carbon and water fluxes at the site level (Figures 2 and 3). In making
622 predictions of the evolution of xylem tension during drought we have significantly advanced
623 the predictive capacity of one state-of-the-art LSM, opening new research avenues to simulate
624 realistic predictions of drought-induced mortality.

625 Our hydraulics approach does have limitations that are pertinent for the LSM community to
626 consider further. First, in order to produce realistic simulations of water potentials, we had to
627 drive CABLE with 30-minute meteorological forcing, requiring us to use a weather generator.
628 At a spatial resolution of 0.05° (~5 km²), these forcing files become significantly larger than
629 files typically used to run offline LSMs. Using a weather generator introduces a new set of
630 biases, for example by muting the diurnal variability in meteorological forcing, which may in
631 turn reduce the intensity of atmospheric drivers during periods of weather extremes.

632 Second, explicit representations of plant hydraulics require additional model parameters, not
633 just the most widely available hydraulic trait, P_{50} (see Table 1). This is the most challenging
634 limitation to LSMs adopting these hydraulics approaches. Where would appropriate
635 parameters come from at the global scale? Particularly, as hydraulic traits have been shown to
636 have similar distributions when re-interpreted not at the species level, but in PFTs more
637 commonly used in LSMs (Konings & Gentine, 2017). Here, we were fortunate to be able to

638 use an existing drought manipulation experiment that considered a wide spectrum of species
639 originating from a marked aridity gradient. In future work we plan to extend this approach,
640 particularly to consider a wider range of species originating from mesic environments. An
641 alternative approach that may reduce the parameterisation burden would be to move towards
642 the new generation of stomatal optimisation models that also account for hydraulic function
643 (Sperry *et al.*, 2017). For example, Sabot *et al.* (2020) recently demonstrated considerable
644 promise applying one of these approaches at the ecosystem-scale, improving model
645 predictions during European droughts. Sabot *et al.* (2020) also proposed a number of
646 simplifications that would make an optimisation approach viable within LSMs.

647 We used a modified version of the Tuzet *et al.* (2003) stomatal model to limit stomatal
648 conductance as a function of Ψ_1 . This approach is attractive as it removes the requirement to
649 assume a minimum Ψ_1 (e.g. Williams *et al.*, 1996; Bonan *et al.*, 2014; Xu *et al.*, 2016), which
650 requires that plants follow isohydric behaviour during water stress, contrary to the emerging
651 literature indicating a broad spectrum of isohydric and anisohydric stomatal behaviour (Klein,
652 2014; Martin-StPaul, 2017). However, using the Tuzet *et al.* (2003) model approach is not
653 without limitations: for example, Yang *et al.* (2019) recently showed it to simulate unrealistic
654 declines in Ψ_1 with increasing vapour pressure deficit, in contrast to experimental
655 observations. This may also explain the discrepancy in sensitivity to water stress shown
656 between model and observations in the flux evaluations (Figures 2 and 3).

657 *Future directions*

658 During the summer of 2019-2020, >5 million ha of forest burnt across South-East Australia
659 (Nolan *et al.*, 2020). The preceding drought which began in 2017, likely played a key role in
660 priming the land surface to burn, due to increased dry fuel litter (leaf and branch shedding). In

661 our first attempt at a hydraulics model for Australia we did not consider the mechanistic
662 turnover of plant tissues, but this is clearly an important future research direction. Xu *et al.*
663 (2016) and Trugman *et al.* (2019) demonstrated promise in dynamically linking leaf
664 phenology to plant hydraulics. Establishing a link between plant hydraulics and leaf shedding
665 (Wolfe *et al.*, 2016) may greatly improve current approaches used to predict the likelihood
666 that the land surface will burn. Existing approaches (e.g. the McArthur Forest Fire Danger
667 Index) make simplistic assumptions about litter and its dryness, meaning that they are over-
668 dependent on fire weather (i.e. temperature-based) metrics.

669 Our model simulations did highlight (Figures 5c and 6b) marked impact of drought across the
670 more mesic northeastern woodlands (forests) of New South Wales, consistent with some of
671 the lowest rainfall totals on record. However, the coastal areas that burnt in the 2019-2020 fire
672 season were not necessarily regions our model highlighted as locations that approached Ψ_{crit} .
673 That is not to say that CABLE did not predict these regions were impacted by drought, but it
674 did not simulate that the drought was extreme enough to induce Ψ_{crit} . Comparing the soil
675 water content for the RF, WSF and DSF regions between the Millennium drought and the Big
676 Dry, shows very similar patterns (cf. Figures 10 and Figures S11). Future model-based work
677 may address the length and severity of water deficit that would be required for more mesic
678 vegetation areas to reach Ψ_{crit} . This could prove important for future land management,
679 particularly given that the Big Dry may have been broken by recent extensive rainfall across
680 South-East Australia, meaning we may not witness water stress thresholds that induce
681 mortality.

682 In our study we assumed that once stomata had closed (“first” drought phase), water
683 continues to be lost at a significantly lower rate via g_{min} (a proxy for stomatal leakiness;
684 “second” drought phase). Extensive measurements of g_{min} are still limited (see Duursma *et al.*,

685 2018 for a review) but some studies have suggested the rate of water loss may have a
686 temperature dependency in some species (Bueno *et al.*, 2019), implying a potentially
687 important interaction during drought. To make these model simulations viable at high-spatial
688 resolution (~5 km), we had to make a series of simplifying assumptions (e.g. that there is
689 xylem refilling (see D. *et al.*, 2018), or additional xylary resistance (see Brodribb &
690 Holbrook, 2004), which require careful evaluation against ground-based data. To bridge this
691 gap, plant water potentials during heatwaves and droughts would be particularly valuable to
692 help constrain model predictions and further develop predictive capacity.

693 **Acknowledgements**

694 MDK, AJP, AMU, MM, MEBS and MR acknowledge support Australian Research Council
695 (ARC) Centre of Excellence for Climate Extremes (CE170100023). MDK, PM, LC and AJP
696 acknowledge support from the ARC Discovery Grant (DP190101823). MDK was also
697 supported from the NSW Research Attraction and Acceleration Program. MEBS also
698 acknowledges support from the UNSW Scientia PhD Scholarship Scheme. This work used
699 eddy covariance data acquired from the OzFlux portal (<http://data.ozflux.org.au/portal/home>).
700 We thank the National Computational Infrastructure at the Australian National University, an
701 initiative of the Australian Government, for access to supercomputer resources. All data
702 analysis and plots were generated using the Python language and the Matplotlib library.

703 **Data Availability Statement**

704 The model source code can be accessed freely after registration at
705 <https://trac.nci.org.au/trac/cable>. All analysis code is freely available from:

706 https://github.com/mdekauwe/SE_AUS_drought_risk_paper.git. In this paper we used
707 CABLE revision 6134. All satellite data used in this manuscript are freely available.

708708

709709

710710

711 **References**

712 **Adams H, Zeppel M, Anderegg W, Hartmann H, Landhäusser S, Tissue D, Huxman T,**
713 **Hudson P, Franz T, Allen C *et al.* 2017.** A multi-species synthesis of physiological
714 mechanisms in drought-induced tree mortality. *Nature Ecology and Evolution* **1**: 1285–1291.

715 **Allen CD, Breshears DD, McDowell NG. 2015.** On underestimation of global vulnerability
716 to tree mortality and forest die-off from hotter drought in the anthropocene. *Ecosphere* **6**:
717 art129.

718 **Anderegg WR, Anderegg LD, Kerr KL, Trugman AT. 2019.** Widespread drought-induced
719 tree mortality at dry range edges indicates climate stress exceeds species' compensating
720 mechanisms. *Global change biology*.

721 **Anderegg WR, Kane JM, Anderegg LD. 2013.** Consequences of widespread tree mortality
722 triggered by drought and temperature stress. *Nature Climate Change* **3**: 30–36.

- 723 **Anderegg W, Schwalm C, Biondi F, Camarero JJ, Koch G, Litvak M, Ogle K, Shaw J,**
724 **Shevliakova E, Williams A *et al.* 2015.** Pervasive drought legacies in forest ecosystems and
725 their implications for carbon cycle models. *Science* **349**: 528–532.
- 726 **Arndt SK, Sanders GJ, Bristow M, Hutley LB, Beringer J, Livesley SJ. 2015.**
727 Vulnerability of native savanna trees and exotic khaya senegalensis to seasonal drought. *Tree*
728 *physiology* **35**: 783–791.
- 729 **Asner GP, Brodrick PG, Anderson CB, Vaughn N, Knapp DE, Martin RE. 2016.**
730 Progressive forest canopy water loss during the 2012–2015 california drought. *Proceedings of*
731 *the National Academy of Sciences* **113**: E249–E255.
- 732 **Bittencourt P, Oliveira R, Costa A da, Giles A, Coughlin I, Costa P, Bartholomew D,**
733 **Ferreira L, Vasconcelos S, Barros F *et al.* 2020.** Amazonian trees have limited capacity to
734 acclimate plant hydraulic properties in response to long-term drought. *Global Change*
735 *Biology*.
- 736 **Blackman CJ, Li X, Choat B, Rymer PD, De Kauwe MG, Duursma RA, Tissue DT,**
737 **Medlyn BE. 2019.** Desiccation time during drought is highly predictable across species of
738 eucalyptus from contrasting climates. *New Phytologist* **224**: 632–643.
- 739 **Bonan G, Williams M, Fisher R, Oleson K. 2014.** Modeling stomatal conductance in the
740 earth system: Linking leaf water-use efficiency and water transport along the soil-plant-
741 atmosphere continuum. *Geoscientific Model Development* **7**: 2193–2222.

- 742 **Bourne AE, Creek D, Peters JM, Ellsworth DS, Choat B. 2017.** Species climate range
743 influences hydraulic and stomatal traits in eucalyptus species. *Annals of Botany* **120**: 123–
744 133.
- 745 **Breshears DD, Cobb NS, Rich PM, Price KP, Allen CD, Balice RG, Romme WH,**
746 **Kastens JH, Floyd ML, Belnap J et al. 2005.** Regional vegetation die-off in response to
747 global-change-type drought. *Proceedings of the National Academy of Sciences* **102**: 15144–
748 15148.
- 749 **Brodribb TJ, Holbrook NM. 2004.** Stomatal protection against hydraulic failure: A
750 comparison of coexisting ferns and angiosperms. *New Phytologist* **162**: 663–670.
- 751 **Bueno A, Alfarhan A, Arand K, Burghardt M, Deininger A-C, Hedrich R, Leide J,**
752 **Seufert P, Staiger S, Riederer M. 2019.** Effects of temperature on the cuticular transpiration
753 barrier of two desert plants with water-spender and water-saver strategies. *Journal of*
754 *experimental botany* **70**: 1613–1625.
- 755 **Campbell GS. 1974.** A simple method for determining unsaturated conductivity from
756 moisture retention data. *Soil science* **117**: 311–314.
- 757 **Carter JL, White DA. 2009.** Plasticity in the huber value contributes to homeostasis in leaf
758 water relations of a mallee eucalypt with variation to groundwater depth. *Tree Physiology* **29**:
759 1407–1418.
- 760 **Choat B, Brodribb TJ, Brodersen CR, Duur, Lopez R, Medlyn BE. 2018.** Triggers of tree
761 mortality under drought. *Nature* **558**: 531–539.

- 762 **Choat B, Jansen S, Brodribb TJ, Cochard H, Delzon S, Bhaskar R, Bucci SJ, Feild TS,**
763 **Gleason SM, Hacke UG *et al.* 2012.** Global convergence in the vulnerability of forests to
764 drought. *Nature* **491**: 752–755.
- 765 **Christoffersen BO, Gloor M, Fauset S, Fyllas NM, Galbraith DR, Baker TR, Kruijt B,**
766 **Rowland L, Fisher RA, Binks OJ *et al.* 2016.** Linking hydraulic traits to tropical forest
767 function in a size-structured and trait-driven model (tfs v. 1-hydro). *Geoscientific Model*
768 *Development* **9**: 4227.
- 769 **Ciais P, Reichstein M, Viovy N, Granier A, Ogee J, Allard V, Aubinet M, Buchmann N,**
770 **Bernhofer C, Carrara A *et al.* 2005.** Europe-wide reduction in primary productivity caused
771 by the heat and drought in 2003. *Nature* **437**: 529–533.
- 772 **Clapp R, Hornberger G. 1978.** Empirical equations for some soil hydraulic properties.
773 *Water resources research* **14**: 601–604.
- 774 **Collins M, Knutti R, Arblaster J, Dufresne J-L, Fichefet T, Friedlingstein P, Gao X,**
775 **Gutowski WJ, Johns T, Krinner G *et al.* 2013.** Long-term climate change: Projections,
776 commitments and irreversibility. In: *Climate change 2013-the physical science basis:*
777 *Contribution of working group i to the fifth assessment report of the intergovernmental panel*
778 *on climate change.* Cambridge University Press, 1029–1136.
- 779 **Cook BI, Ault TR, Smerdon JE. 2015.** Unprecedented 21st century drought risk in the
780 american southwest and central plains. *Science Advances* **1**: e1400082.

- 781 **D. VM, S. SJ, M. LD, H. FE, G. AM, Yujie W, L. AWR. 2018.** A stomatal control model
782 based on optimization of carbon gain versus hydraulic risk predicts aspen sapling responses to
783 drought. *New Phytologist*.
- 784 **Dai A. 2013.** Increasing drought under global warming in observations and models. *Nature*
785 *Climate Change* **3**: 52–58.
- 786 **Davis T, Prentice IC, Stocker B, Thomas R, Whitley R, Wang H, Evans B, Gallego-Sala**
787 **A, Sykes M, Cramer W. 2017.** Simple process-led algorithms for simulating habitats (splash
788 v. 1.0): Robust indices of radiation, evapotranspiration and plant-available moisture.
789 *Geoscientific Model Development* **10**: 689–708.
- 790 **De Kauwe MG, Kala J, Lin Y-S, Pitman AJ, Medlyn BE, Duursma RA, Abramowitz G,**
791 **Wang Y-P, Miralles DG. 2015a.** A test of an optimal stomatal conductance scheme within
792 the CABLE land surface model. *Geoscientific Model Development* **8**: 431–452.
- 793 **De Kauwe M, Zhou S-X, Medlyn B, Pitman A, Wang Y-P, Duursma R, Prentice I.**
794 **2015b.** Do land surface models need to include differential plant species responses to
795 drought? Examining model predictions across a mesic-xeric gradient in europe.
796 *Biogeosciences* **12**: 7503–7518.
- 797 **Decker M, Or D, Pitman A, Ukkola A. 2017.** New turbulent resistance parameterization for
798 soil evaporation based on a pore scale model: Impact on surface fluxes in cable. *Journal of*
799 *Advances in Modeling Earth Systems*.
- 800 **Dijk AI van, Beck HE, Crosbie RS, Jeu RA, Liu YY, Podger GM, Timbal B, Viney NR.**
801 **2013.** The millennium drought in southeast australia (2001–2009): Natural and human causes

802 and implications for water resources, ecosystems, economy, and society. *Water Resources*
803 *Research* **49**: 1040–1057.

804 **Donohue RJ, McVICAR TR, Roderick ML. 2009.** Climate-related trends in australian
805 vegetation cover as inferred from satellite observations, 1981–2006. *Global Change Biology*
806 **15**: 1025–1039.

807 **Du J, Kimball JS, Jones LA, Kim Y, Glassy JM, Watts JD. 2017.** A global satellite
808 environmental data record derived from amsr-e and amsr2 microwave earth observations.
809 *Earth System Science Data* **9**: 791.

810 **Duursma RA, Blackman CJ, Lopéz R, Martin-StPaul NK, Cochard H, Medlyn BE.**
811 **2018.** On the minimum leaf conductance: Its role in models of plant water use, and ecological
812 and environmental controls. *New Phytologist* **0**.

813 **Egea G, Verhoef A, Vidale PL. 2011.** Towards an improved and more flexible
814 representation of water stress in coupled photosynthesis–stomatal conductance models.
815 *Agricultural and Forest Meteorology* **151**: 1370–1384.

816 **Eller CB, Rowland L, Mencuccini M, Rosas T, Williams K, Harper A, Medlyn BE,**
817 **Wagner Y, Klein T, Teodoro GS et al. 2020.** Stomatal optimisation based on xylem
818 hydraulics (sox) improves land surface model simulation of vegetation responses to climate.
819 *New Phytologist* **n/a**.

820 **Fan Y, Miguez-Macho G, Jobbágy EG, Jackson RB, Otero-Casal C. 2017.** Hydrologic
821 regulation of plant rooting depth. *Proceedings of the National Academy of Sciences*:
822 201712381.

- 823 **Fensham R, Holman J. 1999.** Temporal and spatial patterns in drought-related tree dieback
824 in australian savanna. *Journal of Applied Ecology*: 1035–1050.
- 825 **Fensham R, Fairfax R, Ward D. 2009.** Drought-induced tree death in savanna. *Global*
826 *Change Biology* **15**: 380–387.
- 827 **Fisher R, Williams M, COSTA D, Lola A, Malhi Y, Costa R da, Almeida S, Meir P.**
828 **2007.** The response of an eastern amazonian rain forest to drought stress: Results and
829 modelling analyses from a throughfall exclusion experiment. *Global Change Biology* **13**:
830 2361–2378.
- 831 **Fisher, RA, Koven, CD, Anderegg, WRL, et al. 2018.** Vegetation demographics in Earth
832 System Models: A review of progress and priorities. *Global Change Biol.* **24**: 35–54.
- 833 **Galiano L, Martínez-Vilalta J, Lloret F. 2010.** Drought-induced multifactor decline of scots
834 pine in the pyrenees and potential vegetation change by the expansion of co-occurring oak
835 species. *Ecosystems* **13**: 978–991.
- 836 **Gardner WR. 1960.** Dynamic aspects of water availability to plants. *Soil science* **89**: 63–73.
- 837 **Godfree RC, Knerr N, Godfree D, Busby J, Robertson B, Encinas-Viso F. 2019.**
838 Historical reconstruction unveils the risk of mass mortality and ecosystem collapse during
839 pancontinental megadrought. *Proceedings of the National Academy of Sciences*.
- 840 **Griebel A, Bennett LT, Metzen D, Cleverly J, Burba G, Arndt SK. 2016.** Effects of
841 inhomogeneities within the flux footprint on the interpretation of seasonal, annual, and
842 interannual ecosystem carbon exchange. *Agricultural and forest meteorology* **221**: 50–60.

- 843 **Haverd V, Raupach M, Briggs P, Canadell J, Isaac P, Pickett-Heaps C, Roxburgh S,**
844 **Gorsel E van, Viscarra Rossel R, Wang Z. 2013.** Multiple observation types reduce
845 uncertainty in australia's terrestrial carbon and water cycles. *Biogeosciences* **10**: 2011–2040.
- 846 **Haverd V, Smith B, Nieradzik L, Briggs P. 2014.** A stand-alone tree demography and
847 landscape structure module for earth system models: Integration with global forest data.
848 *Biogeosciences* **11**: 2343–2382.
- 849 **Haverd V, Smith B, Nieradzik L, Briggs PR, Woodgate W, Trudinger CM, Canadell JG.**
850 **2018.** A new version of the cable land surface model (subversion revision r4601)
851 incorporating land use and land cover change, woody vegetation demography, and a novel
852 optimisation-based approach to plant coordination of photosynthesis. *Geoscientific Model*
853 *Development* **11**: 2995–3026.
- 854 **Hengl T, Jesus JM de, Heuvelink GB, Gonzalez MR, Kilibarda M, Blagotić A,**
855 **Shangguan W, Wright MN, Geng X, Bauer-Marschallinger B et al. 2017.** SoilGrids250m:
856 Global gridded soil information based on machine learning. *PLoS one* **12**.
- 857 **Hill T, Williams M, Woodward F, Moncrieff J. 2011.** Constraining ecosystem processes
858 from tower fluxes and atmospheric profiles. *Ecological Applications* **21**: 1474–1489.
- 859 **Hopkins ER. 1973.** Eucalypt dieback inAustralia. In: C. MG, Idczak RM, eds. Victoria:
860 Forests Comission, 1–16.
- 861 **Horst SVJ van der, Pitman AJ, De Kauwe MG, Ukkola A, Abramowitz G, Isaac P. 2019.**
862 How representative are fluxnet measurements of surface fluxes during temperature extremes?
863 *Biogeosciences* **16**: 1829–1844.

- 864 **Isaac P, Cleverly J, McHugh I, Van Gorsel E, Ewenz C, Beringer J. 2017.** OzFlux data:
865 Network integration from collection to curation. *Biogeosciences* **14**: 2903–2928.
- 866 **Jiang M, Medlyn BE, Drake JE, Duursma RA, Anderson IC, Barton CVM, Boer MM,**
867 **Carrillo Y, Castañeda-Gómez L, Collins L et al. 2020.** The fate of carbon in a mature forest
868 under carbon dioxide enrichment. *Nature* **580**: 227–231.
- 869 **Jiang M, Zaehle S, De Kauwe MG, Walker AP, Caldararu S, Ellsworth DS, Medlyn BE.**
870 **2019.** The quasi-equilibrium framework revisited: Analyzing long-term enrichment responses
871 in plant–soil models. *Geoscientific Model Development* **5**: 2069–2089.
- 872 **Jones DA, Wang W, Fawcett R. 2009.** High-quality spatial climate data-sets for australia.
873 *Australian Meteorological and Oceanographic Journal* **58**: 233.
- 874 **Jump AS, Ruiz-Benito P, Greenwood S, Allen CD, Kitzberger T, Fensham R, Martínez-**
875 **Vilalta J, Lloret F. 2017.** Structural overshoot of tree growth with climate variability and the
876 global spectrum of drought-induced forest dieback. *Global change biology* **23**: 3742–3757.
- 877 **Keith H, Van Gorsel E, Jacobsen KL, Cleugh HA. 2012.** Dynamics of carbon exchange in
878 a eucalyptus forest in response to interacting disturbance factors. *Agricultural and Forest*
879 *Meteorology* **153**: 67–81.
- 880 **Kelly JW, Duursma RA, Atwell BJ, Tissue DT, Medlyn BE. 2016.** Drought × co₂
881 interactions in trees: A test of the low-intercellular co₂ concentration (ci) mechanism. *New*
882 *Phytologist* **209**: 1600–1612.

- 883 **Kennedy D, Swenson S, Oleson KW, Fisher RA, Lawrence DM, Costa ACL da, Gentine**
884 **P. 2019.** Implementing plant hydraulics in the community land model, version 5. *Journal of*
885 *Advances in Modeling Earth Systems*.
- 886 **Klein T. 2014.** The variability of stomatal sensitivity to leaf water potential across tree
887 species indicates a continuum between isohydric and anisohydric behaviours. *Functional*
888 *Ecology* **28**: 1313–1320.
- 889 **Konings AG, Gentine P. 2017.** Global variations in ecosystem-scale isohydricity. *Global*
890 *Change Biology* **23**: 891–905.
- 891 **Kowalczyk E, Stevens L, Law R, Dix M, Wang Y, Harman I, Haynes K, Srbinovsky J,**
892 **Pak B, Ziehn T. 2013.** The land surface model component of access: Description and impact
893 on the simulated surface climatology. *Aust Meteorol Oceanogr J* **63**: 65–82.
- 894 **Kowalczyk EA, Wang YP, Wang P, Law RH, Davies HL. 2006.** *The csiro atmosphere*
895 *biosphere land exchange (CABLE) model for use in climate models and as an offline model.*
896 CSIRO.
- 897 **Lamy J-B, Delzon S, Bouche PS, Alia R, Vendramin GG, Cochard H, Plomion C. 2014.**
898 Limited genetic variability and phenotypic plasticity detected for cavitation resistance in a m
899 editerranean pine. *New Phytologist* **201**: 874–886.
- 900 **Landsberg J. 1985.** Drought and dieback of rural eucalypts. *Austral Ecology* **10**: 87–90.
- 901 **Li X, Blackman CJ, Choat B, Duursma RA, Rymer PD, Medlyn BE, Tissue DT. 2018.**
902 Tree hydraulic traits are co-ordinated and strongly linked to climate-of-origin across a rainfall
903 gradient.

- 904 **Li X, Chris BJ, Peters JM, Choat B, Rymer PD, Medlyn BE, Tissue DT. 2019.** More than
905 iso/anisohdry: Hydroscares integrate plant water-use and drought tolerance traits in ten
906 eucalypt species from contrasting climates. *Functional Ecology*.
- 907 **Li S, Feifel M, Karimi Z, Schuldt B, Choat B, Jansen S. 2015.** Leaf gas exchange
908 performance and the lethal water potential of five european species during drought. *Tree*
909 *physiology* **36**: 179–192.
- 910 **Liu YY, Jeu RA de, McCabe MF, Evans JP, Dijk AI van. 2011.** Global long-term passive
911 microwave satellite-based retrievals of vegetation optical depth. *Geophysical Research*
912 *Letters* **38**.
- 913 **Lorenz R, Pitman A, Donat M, Hirsch A, Kala J, Kowalczyk E, Law R, Srbinovsky J.**
914 **2014.** Representation of climate extreme indices in the access1. 3b coupled atmosphere-land
915 surface model. *Geoscientific Model Development* **7**: 545–567.
- 916 **Martin-StPaul NK et a. 2017.** Plant resistance to drought depends on timely stomatal
917 closure. *Ecology Letters*.
- 918 **McDowell NG, Fisher RA, Xu C, Domec J, Hölttä T, Mackay DS, Sperry JS, Boutz A,**
919 **Dickman L, Gehres N et al. 2013.** Evaluating theories of drought-induced vegetation
920 mortality using a multimodel–experiment framework. *New Phytologist*.
- 921 **McVicar TR. 2011.** Near-surface wind speed for australia. V10. Data collection.
- 922 **McVicar TR, Van Niel TG, Li LT, Roderick ML, Rayner DP, Ricciardulli L, Donohue**
923 **RJ. 2008.** Wind speed climatology and trends for australia, 1975–2006: Capturing the stilling

- 924 phenomenon and comparison with near-surface reanalysis output. *Geophysical Research*
925 *Letters* **35**.
- 926 **Medlyn BE, De Kauwe MG, Zaehle S, Walker AP, Duursma RA, Luus K, Mishurov M,**
927 **Pak B, Smith B, Wang Y-P et al. 2016.** Using models to guide field experiments: A priori
928 predictions for the CO₂ response of a nutrient-and water-limited native eucalypt woodland.
929 *Global Change Biology* **22**: 2834–2851.
- 930 **Mencuccini M, Minunno F, Salmon Y, Martínez-Vilalta J, Hölttä T. 2015.** Coordination
931 of physiological traits involved in drought-induced mortality of woody plants. *New*
932 *Phytologist* **in press**.
- 933 **Mitchell P, O’Grady A, Tissue D, Worledge D, Pinkard E. 2014.** Co-ordination of growth,
934 gas exchange and hydraulics define the carbon safety margin in tree species with contrasting
935 drought strategies. *Tree physiology* **34**: 443–458.
- 936 **Moore GW, Edgar CB, Vogel JG, Washington-Allen RA, March RG, Zehnder R. 2016.**
937 Tree mortality from an exceptional drought spanning mesic to semiarid ecoregions.
938 *Ecological Applications* **26**: 602–611.
- 939 **Mueller RC, Scudder CM, Porter ME, Talbot Trotter III R, Gehring CA, Whitham TG.**
940 **2005.** Differential tree mortality in response to severe drought: Evidence for long-term
941 vegetation shifts. *Journal of Ecology* **93**: 1085–1093.
- 942 **Myers BA, Neales T. 1984.** Seasonal changes in the water relations of eucalyptus behriana f.
943 Muell. And e. Microcarpa (maiden) maiden in the field. *Australian Journal of Botany* **32**:
944 495–510.

- 945 **Nepstad DC, Tohver IM, Ray D, Moutinho P, Cardinot G. 2007.** Mortality of large trees
946 and lianas following experimental drought in an amazon forest. *Ecology* **88**: 2259–2269.
- 947 **Neumann M, Mues V, Moreno A, Hasenauer H, Seidl R. 2017.** Climate variability drives
948 recent tree mortality in europe. *Global change biology* **23**: 4788–4797.
- 949 **Nolan RH, Boer MM, Collins L, Resco de Dios V, Clarke H, Jenkins M, Kenny B,**
950 **Bradstock RA. 2020.** Causes and consequences of eastern australia’s 2019-20 season of
951 mega-fires. *Global change biology*.
- 952 **Nolan RH, Mitchell PJ, Bradstock RA, Lane PN. 2014.** Structural adjustments in
953 resprouting trees drive differences in post-fire transpiration. *Tree physiology* **34**: 123–136.
- 954 **Ogle K. 2009.** Hierarchical bayesian statistics: Merging experimental and modeling
955 approaches in ecology. *Ecological Applications* **19**: 577–581.
- 956 **Peñuelas J, Canadell J, Ogaya R. 2011.** Increased water-use efficiency during the 20th
957 century did not translate into enhanced tree growth. *Global Ecology and Biogeography* **20**:
958 597–608.
- 959 **Phillips RP, Bernhardt ES, Schlesinger WH. 2009.** Elevated CO₂ increases root exudation
960 from loblolly pine (*pinus taeda*) seedlings as an n-mediated response. *Tree Physiology* **29**:
961 1513–1523.
- 962 **Phillips OL, Van Der Heijden G, Lewis SL, López-González G, Aragão LE, Lloyd J,**
963 **Malhi Y, Monteagudo A, Almeida S, Dávila EA et al. 2010.** Drought–mortality
964 relationships for tropical forests. *New Phytologist* **187**: 631–646.

- 965 **Pitman A, Avila F, Abramowitz G, Wang Y, Phipps S, Noblet-Ducoudré N de. 2011.**
966 Importance of background climate in determining impact of land-cover change on regional
967 climate. *Nature Climate Change* **1**: 472–475.
- 968 **Pook E. 1986.** Canopy dynamics of eucalyptus maculata hook. IV. Contrasting responses to
969 two severe droughts. *Australian journal of botany* **34**: 1–14.
- 970 **Powell TL, Galbraith DR, Christoffersen BO, Harper A, Imbuzeiro HMA, Rowland L,**
971 **Almeida S, Brando PM, Costa ACL da, Costa MH et al. 2013.** Confronting model
972 predictions of carbon fluxes with measurements of amazon forests subjected to experimental
973 drought. *New Phytologist* **200**: 350–365.
- 974 **Priestley CHB, Taylor R. 1972.** On the assessment of surface heat flux and evaporation
975 using large-scale parameters. *Monthly weather review* **100**: 81–92.
- 976 **Raupach M. 1994.** Simplified expressions for vegetation roughness length and zero-plane
977 displacement as functions of canopy height and area index. *Boundary-Layer Meteorology* **71**:
978 211–216.
- 979 **Raupach M, Finkele K, Zhang L. 1997.** SCAM (soil-canopy-atmosphere model):
980 Description and comparison with field data. *Aspendale, Australia: CSIRO CEM Technical*
981 *Report*: 81.
- 982 **Reichstein M, Bahn M, Ciais P, Frank D, Mahecha MD, Seneviratne SI, Zscheischler J,**
983 **Beer C, Buchmann N, Frank DC et al. 2013.** Climate extremes and the carbon cycle. *Nature*
984 **500**: 287–295.

- 985 **Ross C, Brack C. 2015.** Eucalyptus viminalis dieback in the monaro region, nsw. *Australian*
986 *forestry* **78**: 243–253.
- 987 **Rowland L, Costa ACL da, Galbraith DR, Oliveira RS, Binks OJ, Oliveira AAR, Pullen**
988 **AM, Doughty CE, Metcalfe DB, Vasconcelos SS et al. 2015.** Death from drought in tropical
989 forests is triggered by hydraulics not carbon starvation. *Nature* **528**: 119–122.
- 990 **Ruiz-Benito P, Madrigal-Gonzalez J, Ratcliffe S, Coomes DA, Kändler G, Lehtonen A,**
991 **Wirth C, Zavala MA. 2014.** Stand structure and recent climate change constrain stand basal
992 area change in european forests: A comparison across boreal, temperate, and mediterranean
993 biomes. *Ecosystems* **17**: 1439–1454.
- 994 **Ruthrof K, Matusick G, Hardy G. 2015.** Early differential responses of co-dominant
995 canopy species to sudden and severe drought in a mediterranean-climate type forest. *Forests*
996 **6**: 2082–2091.
- 997 **Saatchi S, Asefi-Najafabady S, Malhi Y, Aragão L, Anderson L, Myneni R, Nemani R.**
998 **2013.** Persistent effects of a severe drought on amazonian forest canopy. *Proceedings of the*
999 *National Academy of Sciences* **110**: 565–570.
- 1000 **Sabot ME, De Kauwe MG, Pitman AJ, Medlyn BE, Verhoef A, Ukkola AM,**
1001 **Abramowitz G. 2020.** Plant profit maximisation improves predictions of european forest
1002 responses to drought. *New Phytologist*.
- 1003 **Schwarz PA, Law BE, Williams M, Irvine J, Kurpius M, Moore D. 2004.** Climatic versus
1004 biotic constraints on carbon and water fluxes in seasonality drought-affected ponderosa pine
1005 ecosystems, *Global Biogeochemical Cycles* **18**: GB4007, doi:10.1029/2004GB002234.

- 1006 **Service UF. 2016.** *USDA forest service pacific southwest region. Aerial detection surveys*
1007 *report: Summary for may 15–19 report no. Fseprd506698.* USDA Forest Service.
- 1008 **Simard M, Pinto N, Fisher JB, Baccini A. 2011.** Mapping forest canopy height globally
1009 with spaceborne lidar. *Journal of Geophysical Research: Biogeosciences* **116**: G04021.
- 1010 **Sperry JS, Tyree MT. 1988.** Mechanism of water stress-induced xylem embolism. *Plant*
1011 *Physiology* **88**: 581–587.
- 1012 **Sperry JS, Venturas MD, Anderegg WR, Mencuccini M, Mackay DS, Wang Y, Love**
1013 **DM. 2017.** Predicting stomatal responses to the environment from the optimization of
1014 photosynthetic gain and hydraulic cost. *Plant, Cell & Environment* **40**: 816–830.
- 1015 **Stoneman G. 1994.** Ecology and physiology of establishment of eucalypt seedlings from
1016 seed: A review. *Australian Forestry* **57**: 11–29.
- 1017 **Trenberth KE, Dai A, Van Der Schrier G, Jones PD, Barichivich J, Briffa KR, Sheffield**
1018 **J. 2014.** Global warming and changes in drought. *Nature Climate Change* **4**: 17–22.
- 1019 **Trugman A, Anderegg L, Wolfe B, Birami B, Ruehr N, Detto M, Bartlett M, Anderegg**
1020 **W. 2019.** Climate and plant trait strategies determine tree carbon allocation to leaves and
1021 mediate future forest productivity. *Global change biology*.
- 1022 **Tuzet A, Perrier A, Leuning R. 2003.** A coupled model of stomatal conductance,
1023 photosynthesis and transpiration. *Plant, Cell & Environment* **26**: 1097–1116.
- 1024 **Ukkola A, De Kauwe MG, Pitman AJ, Best MJ, Haverd V, M. D, G. A, Haughton N.**
1025 **2016a.** Land surface models systematically overestimate the intensity, duration and

- 1026 magnitude of seasonal-scale evaporative droughts. In review. *Environmental Research Letters*
1027 **11**: 104012.
- 1028 **Ukkola AM, Haughton N, De Kauwe MG, Abramowitz G, Pitman AJ. 2017.** FluxnetLSM
1029 R package (v1.0): A community tool for processing fluxnet data for use in land surface
1030 modelling. *Geoscientific Model Development* **10**: 3379–3390.
- 1031 **Ukkola AM, Pitman AJ, Decker M, De Kauwe MG, Abramowitz G, Kala J, Wang Y-P.**
1032 **2016b.** Modelling evapotranspiration during precipitation deficits: Identifying critical
1033 processes in a land surface model. *Hydrology and Earth System Sciences* **20**: 2403–2419.
- 1034 **Urli M, Porté AJ, Cochard H, Guengant Y, Burlett R, Delzon S. 2013.** Xylem embolism
1035 threshold for catastrophic hydraulic failure in angiosperm trees. *Tree physiology* **33**: 672–683.
- 1036 **Vermote E. 2019.** NOAA climate data record (cdr) of avhrr surface reflectance, version 5.
- 1037 **Wang Y, Leuning R. 1998.** A two-leaf model for canopy conductance, photosynthesis and
1038 partitioning of available energy i::: Model description and comparison with a multi-layered
1039 model. *Agricultural and Forest Meteorology* **91**: 89–111.
- 1040 **Wang YP, Kowalczyk E, Leuning R, Abramowitz G, Raupach MR, Pak B, Gorsel E**
1041 **van, Luhar A. 2011.** Diagnosing errors in a land surface model (CABLE) in the time and
1042 frequency domains. *Journal of Geophysical Research: Biogeosciences (2005–2012)* **116**.
- 1043 **Wang YP, Law RM, Pak B. 2010.** A global model of carbon, nitrogen and phosphorus
1044 cycles for the terrestrial biosphere. *Biogeosciences* **7**: 2261–2282.

- 1045 **Weed AS, Ayres MP, Hicke JA. 2013.** Consequences of climate change for biotic
1046 disturbances in north american forests. *Ecological Monographs* **83**: 441–470.
- 1047 **Whittaker R, Niering W, Crisp M. 1979.** Structure, pattern, and diversity of a mallee
1048 community in new south wales. *Vegetatio* **39**: 65–76.
- 1049 **Wigneron J-P, Fan L, Ciais P, Bastos A, Brandt M, Chave J, Saatchi S, Baccini A,**
1050 **Fensholt R. 2020.** Tropical forests did not recover from the strong 2015–2016 el niño event.
1051 *Science advances* **6**: eaay4603.
- 1052 **Williams AP, Allen CD, Macalady AK, Griffin D, Woodhouse CA, Meko DM, Swetnam**
1053 **TW, Rauscher SA, Seager R, Grissino-Mayer HD et al. 2013.** Temperature as a potent
1054 driver of regional forest drought stress and tree mortality. *Nature climate change* **3**: 292–297.
- 1055 **Williams M, Bond B, Ryan M. 2001a.** Evaluating different soil and plant hydraulic
1056 constraints on tree function using a model and sap flow data from ponderosa pine. *Plant, Cell*
1057 *& Environment* **24**: 679–690.
- 1058 **Williams M, Law BE, Anthoni PM, Unsworth MH. 2001b.** Use of a simulation model and
1059 ecosystem flux data to examine carbon-water interactions in ponderosa pine. *Tree physiology*
1060 **21**: 287–298.
- 1061 **Williams M, Rastetter EB, Fernandes DN, Goulden ML, Wofsy SC, Shaver GR and.**
1062 **1996.** Modelling the soil-plant-atmosphere continuum in a quercus-acer stand at harvard
1063 forest: The regulation of stomatal conductance by light, nitrogen and soil/plant hydraulic
1064 properties. *Plant, Cell and Environment* **19**: 911–927.

1065 **Wolfe BT, Sperry JS, Kursar TA. 2016.** Does leaf shedding protect stems from cavitation
 1066 during seasonaldroughts? A test of the hydraulic fuse hypothesis. *New Phytologist* **212**: 1007–
 1067 1018.

1068 **Xu X, Medvigy D, Powers JS, Becknell JM, Guan K. 2016.** Diversity in plant hydraulic
 1069 traits explains seasonal and inter-annual variations of vegetation dynamics in seasonally dry
 1070 tropical forests. *New Phytologist* **212**: 80–95.

1071 **Yang J, Duursma R, De Kauwe M, Kumarathunge D, Jiang M, Mahmud K, Gimeno T,**
 1072 **Crous K, Ellsworth D, Peters J et al. 2019.** Incorporating non-stomatal limitation improves
 1073 the performance of leaf and canopy models at high vapour pressure deficit. *Tree Physiology*
 1074 **39**: 1961–1974.

1075 **Zhou S, Duursma RA, Medlyn BE, Kelly JW, Prentice IC. 2013.** How should we model
 1076 plant responses to drought? An analysis of stomatal and non-stomatal responses to water
 1077 stress. *Agricultural and Forest Meteorology* **182-183**: 204–214.

1078 **Figure Captions**

1079 Figure 1: Probability density and histograms showing the time taken to reach the point of
 1080 hydraulic failure (Ψ_{crit}) for each of the five vegetation classes in the absence of precipitation,
 1081 with a constant air temperature of 35°C and a relative humidity of 10%. For each vegetation
 1082 class, the (horizontal) spread in the time taken to reach hydraulic failure relates to resilience
 1083 inferred from sampling all possible photosynthetic (e.g. V_{cmax}), hydraulic (e.g. P_{50}) and
 1084 structural (LAI) traits. The vegetation classes shown are: Rainforest (RAF), Wet sclerophyll
 1085 forest (WSF), Dry sclerophyll forest (DSF), Grassy Woodland (GRW) and Semi-arid

1086 woodland (SAW). For each vegetation class, the curved line shows the fitted kernel density
1087 estimate (KDE).

1088 Figure 2: A comparison between fluxes simulated by the Control and Hydraulics model for
1089 gross primary productivity (GPP) and latent heat flux (LE) at the Wombat State Forest
1090 FLUXNET site during a pronounced period of water stress. The data have been smoothed
1091 with a 5-day moving window to aid visualisation.

1092 Figure 3: A comparison between fluxes simulated by the Control and Hydraulics model for
1093 gross primary productivity (GPP) and latent heat flux (LE) at the Tumbarumba FLUXNET
1094 site during a pronounced period of water stress. The data have been smoothed with a 5-day
1095 moving window to aid visualisation.

1096 Figure 4: Average climatic water deficit: precipitation (P) minus potential evapotranspiration
1097 (PET) (a) prior to the Millennium Drought (1990–2000) and (b) the difference: during the
1098 Millennium Drought minus prior for South-East Australia.

1099 Figure 5: Average climatic water deficit: precipitation (P) minus actual evapotranspiration
1100 (AET) (a) simulated by CABLE-hydraulics for (a) Millennium Drought (2000–2009) and (b)
1101 the Big Dry (2017–2019).

1102 Figure 6: Maximum percentage loss of hydraulic conductivity (%) simulated by CABLE
1103 during (a) the Millennium drought (2000–2009) and (b) the Big Dry (2017–2019) (panel b).
1104 Ψ_{crit} is the xylem pressure inducing a 88 % hydraulic conductivity.

1105 Figure 7: Remotely sensed map of the relative percentage difference between: (a) the mean
1106 summer (December–February) vegetation optical depth (VOD) during the Millennium

1107 drought (2000–2009) relative to 1993–2000 and (b) the mean summer VOD during the Big
1108 Dry (2017–2018) relative to 1993–2016. Note we do not include the final summer 2019 due
1109 to the confounding impact of fires across South-East Australia.

1110 Figure 8: Remotely sensed map of the relative percentage difference between: (a) the mean
1111 summer normalised difference vegetation index (NDVI) during the Millennium drought
1112 (2000–2009) relative to 1993–2000 and (b) the mean summer NDVI during the Big Dry
1113 (2017–2018) relative to 1993–2016. Note we do not include summer 2019 due to the
1114 confounding impact of fires across South-East Australia.

1115 Figure 9: Timeseries of the percentage loss of hydraulic conductivity (%) for each of the five
1116 vegetation classes during (a) the Millennium drought and (b) Big Dry. For each vegetation
1117 class, the line shows the spatial average across all pixels. The vegetation classes shown are:
1118 Rainforest (RAF), Wet sclerophyll forest (WSF), Dry sclerophyll forest (DSF), Grassy
1119 Woodland (GRW) and Semi-arid woodland (SAW).

1120 Figure 10: Sensitivity of percentage loss of hydraulic conductivity (%) to soil water
1121 availability in the top four soil layers (0.64 m, 80% of roots) for each vegetation class during
1122 the Millennium drought. The vegetation classes shown are: Rainforest (RAF), Wet
1123 sclerophyll forest (WSF), Dry sclerophyll forest (DSF), Grassy Woodland (GRW) and Semi-
1124 arid woodland (SAW). Ψ_{crit} is the xylem pressure inducing a 88 % hydraulic conductivity.

1125 Supplementary Figure 1: South-East Australia's July to June annual rainfall during the
1126 Millennium drought (2000–2009) relative to historic records (1900–2018). Maps show each
1127 year's rainfall ranked against historic records expressed as a percentile.

1128 Supplementary Figure 2: South-East Australia's July to June annual rainfall during the Big
1129 Dry (2016–2018) relative to historic records (1900–2018). Maps show each year's rainfall
1130 ranked against historic records expressed as a percentile.

1131 Supplementary Figure 3: Study area in South-East Australia.

1132 Supplementary Figure 4: New tree landcover map for South-East Australia, classified from
1133 the National Vegetation Information System's distribution of vegetation types in Australian
1134 landscapes. The legend shows: Rainforest (RAF), Wet sclerophyll forest (WSF), Dry
1135 sclerophyll forest (DSF), Grassy Woodland (GRW) and Semi-arid woodland (SAW).

1136 Supplementary Figure 5: Water stress modifiers used in CABLE shown as: (a) a function of
1137 volumetric soil moisture content in the Control model and (b) (leaf and stem) water potential
1138 in the Hydraulics model. In the Control model, the water stress modifier limits canopy gas
1139 exchange, whereas in the hydraulics model Ψ_l limits stomatal conductance as a function of
1140 leaf water potential and Ψ_x limits whole-plant hydraulic conductance as a function of stem
1141 water potential. In the Control model, the water stress sensitivity is shown for a sand soil and
1142 in the Hydraulics model, the sensitivities are shown for the wet sclerophyll forest vegetation
1143 class.

1144 Supplementary Figure 6: Modelled pre-dawn weighted soil (Ψ_{sw}), midday leaf (Ψ_l) and
1145 midday stem (Ψ_x) water potentials at the Wombat State Forest FLUXNET site during a
1146 pronounced period of water stress.

1147 Supplementary Figure 7: Modelled pre-dawn weighted soil (Ψ_{sw}), midday leaf (Ψ_l) and
1148 midday stem (Ψ_x) water potentials at the Tumbarumba FLUXNET site during a pronounced
1149 period of water stress.

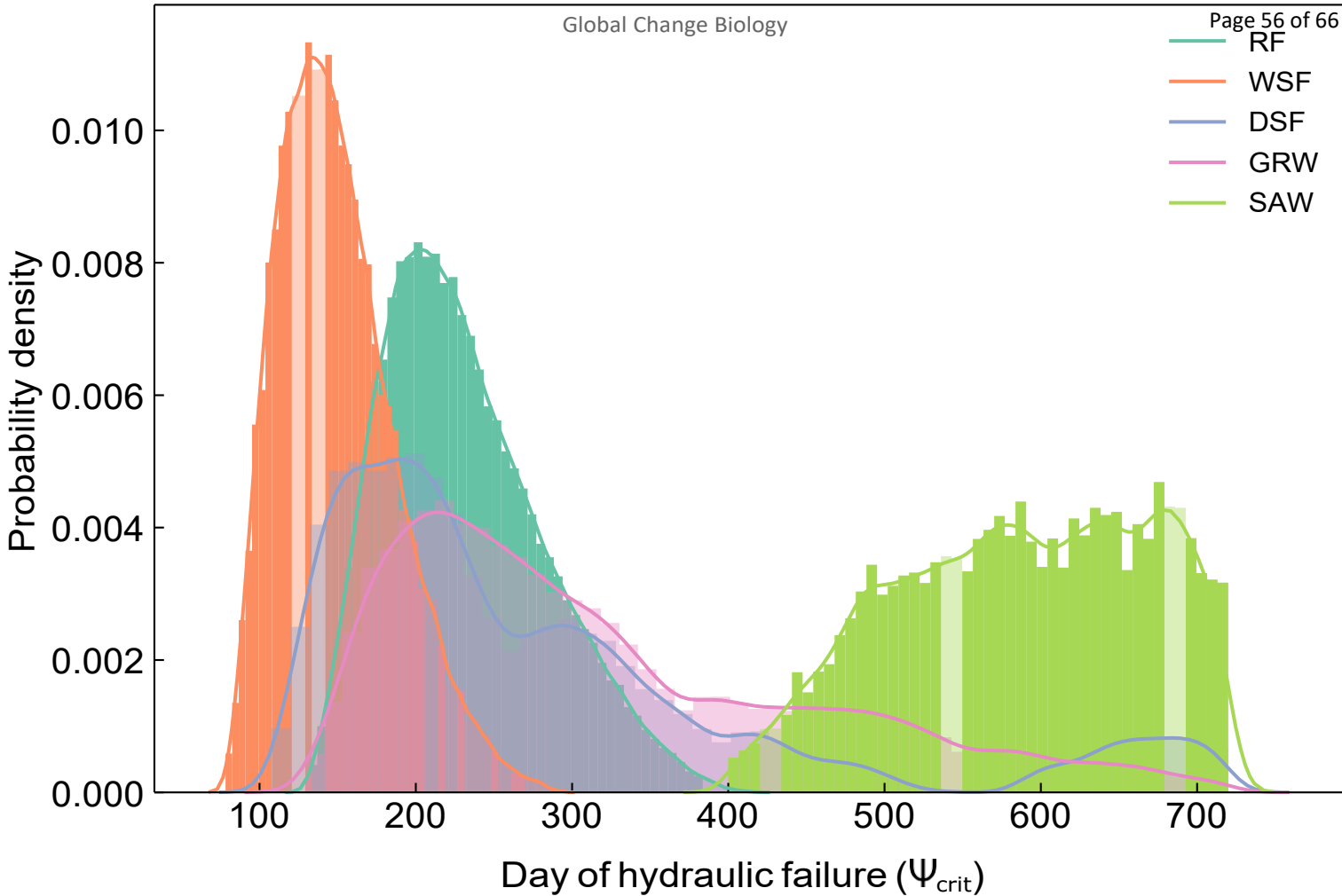
1150 Supplementary Figure 8: Remotely sensed map of the relative percentage difference between:
1151 (a) the lowest summer (December–February) vegetation optical depth (VOD) during the
1152 Millennium drought (2000–2009) relative to 1993–2000 and (b) the mean summer VOD
1153 during the Big Dry (2017–2018) relative to 1993–2016. Note we do not include the final
1154 summer 2019 due to the confounding impact of fires across South-East Australia.

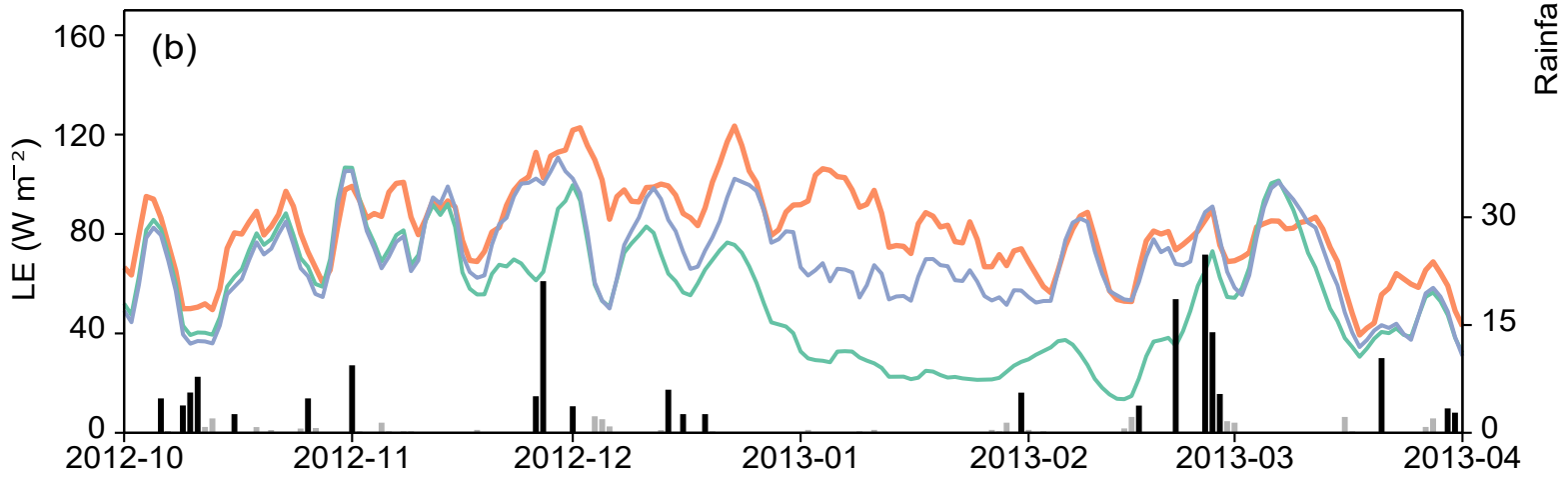
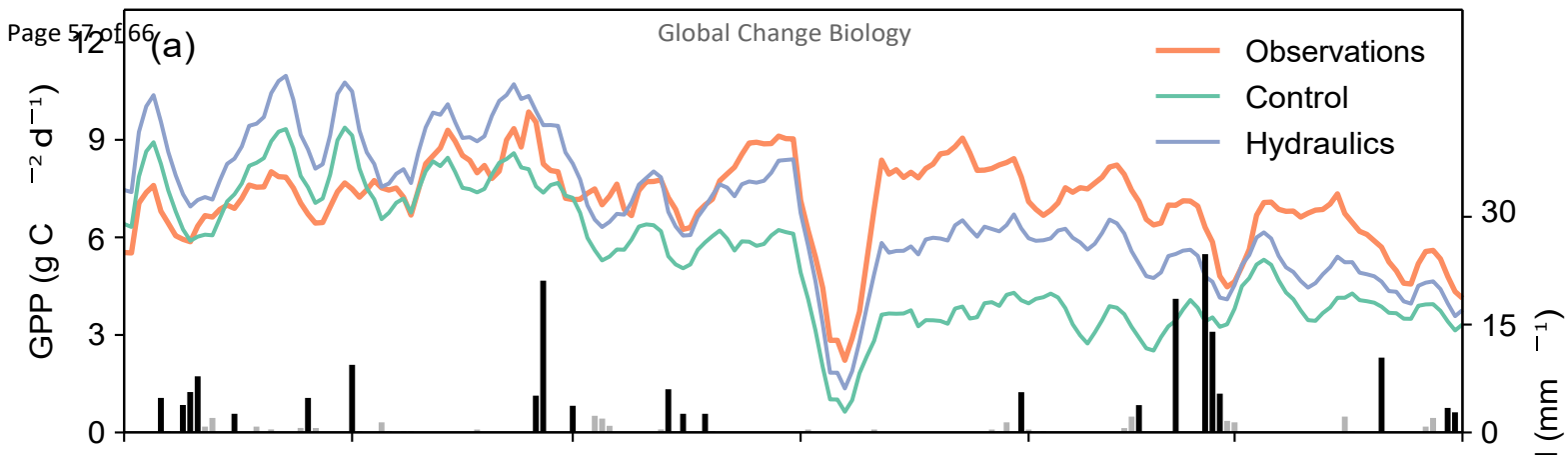
1155 Supplementary Figure 9: Remotely sensed map of the relative percentage difference between:
1156 (a) the lowest summer normalised difference vegetation index (NDVI) during the Millennium
1157 drought (2000–2009) relative to 1993–2000 and (b) the mean summer NDVI during the Big
1158 Dry (2017–2018) relative to 1993–2016. Note we do not include summer 2019 due to the
1159 confounding impact of fires across South-East Australia.

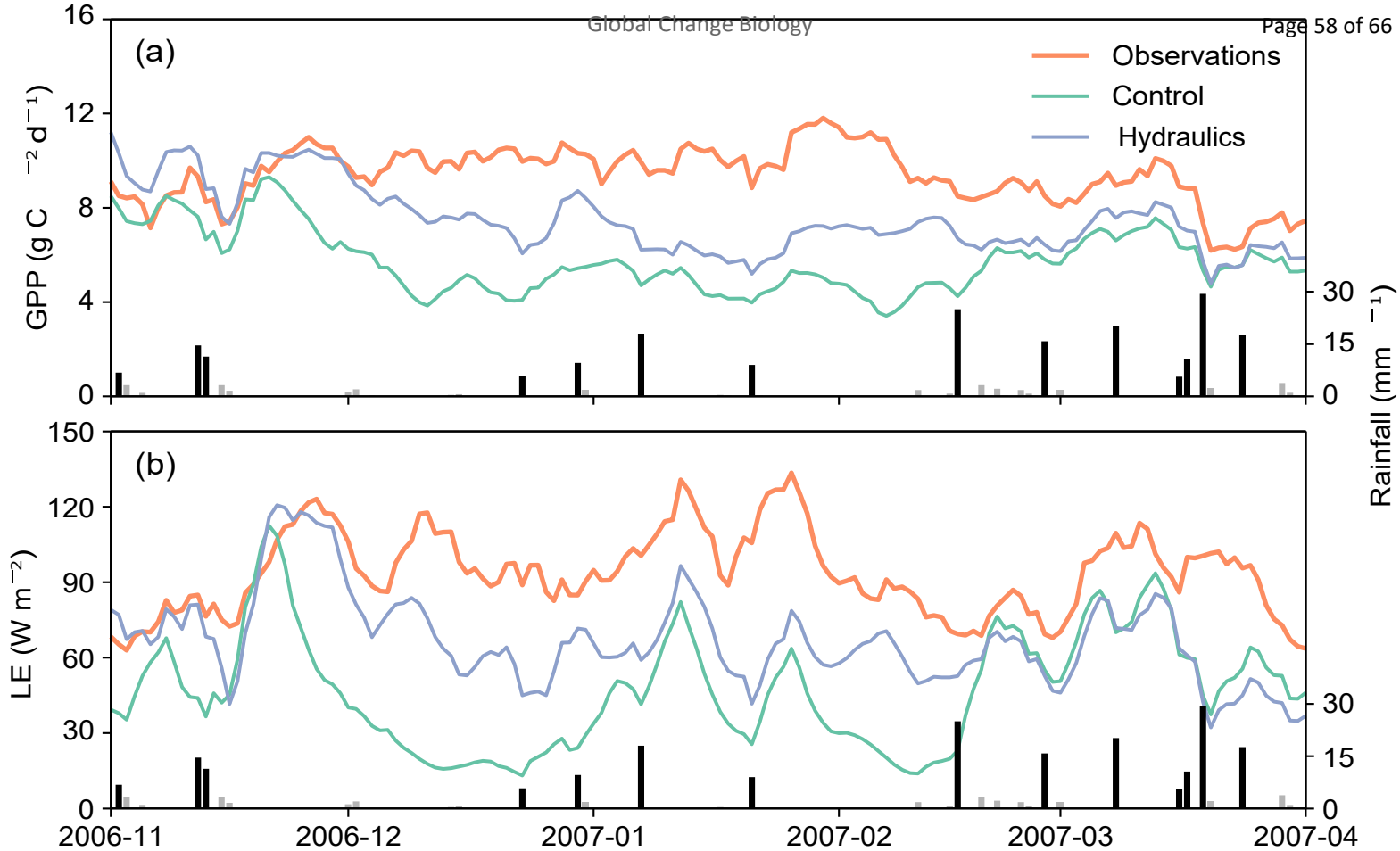
1160 Supplementary Figure 10: Modelled pre-dawn weighted soil (Ψ_{sw}), pre-dawn stem (Ψ_x) and
1161 midday leaf (Ψ_l) water potentials for two representative Grassy Woodland (GRW) (panels a
1162 and b) pixels and two representative Semi-arid woodland (SAW) (panels c and d) pixels
1163 during the Big Dry (2016–2019). Note the difference in trajectories between panels c and d
1164 relates to differences in leaf area index: 0.22 m² m⁻² (c) vs 1.6 m² m⁻² (d).

1165 Supplementary Figure 11: Sensitivity of percentage loss of hydraulic conductivity (%) to soil
1166 water availability in the top four soil layers (0.64 m, 80% of roots) for each vegetation class
1167 during the Big Dry. The vegetation classes shown are: Rainforest (RAF), Wet sclerophyll
1168 forest (WSF), Dry sclerophyll forest (DSF), Grassy Woodland (GRW) and Semi-arid
1169 woodland (SAW). Ψ_{crit} is the xylem pressure inducing a 88 % hydraulic conductivity.

1170







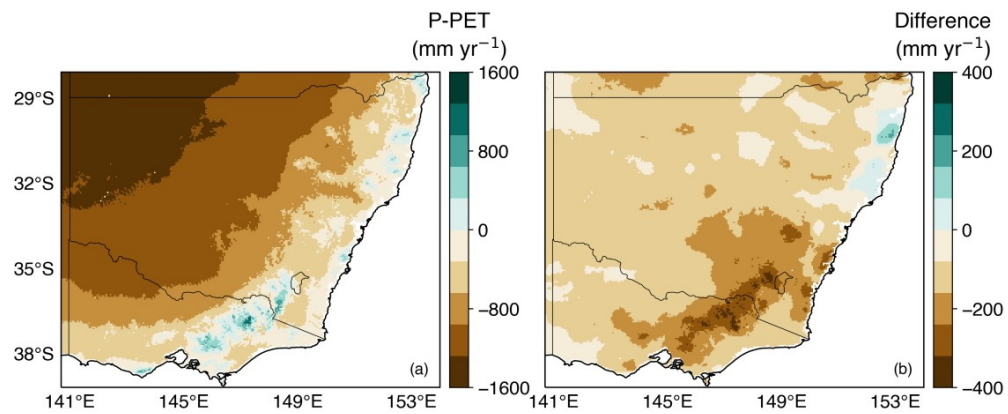


Figure 4: Average climatic water deficit: precipitation (P) minus potential evapotranspiration (PET) (a) prior to the Millennium Drought (1990–2000) and (b) the difference: during the Millennium Drought minus prior for South-East Australia.

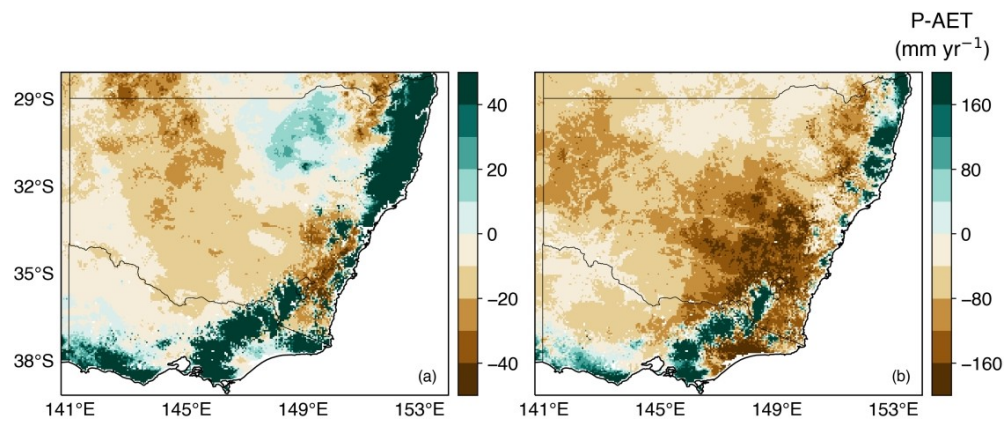


Figure 5: Average climatic water deficit: precipitation (P) minus actual evapotranspiration (AET) (a) simulated by CABLE-hydraulics for (a) Millennium Drought (2000–2009) and (b) the Big Dry (2017–2019).

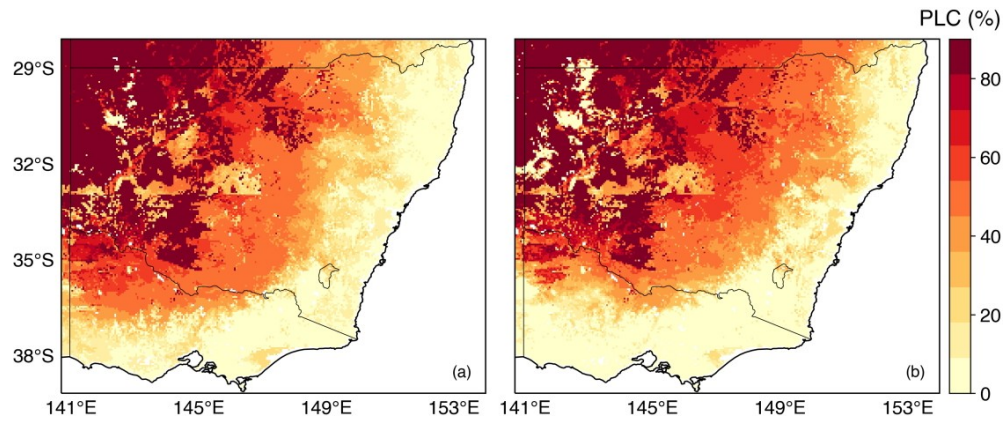


Figure 6: Maximum percentage loss of hydraulic conductivity (%) simulated by CABLE during (a) the Millennium drought (2000–2009) and (b) the Big Dry (2017–2019) (panel b). Ψ_{crit} is the xylem pressure inducing a 88 % hydraulic conductivity.

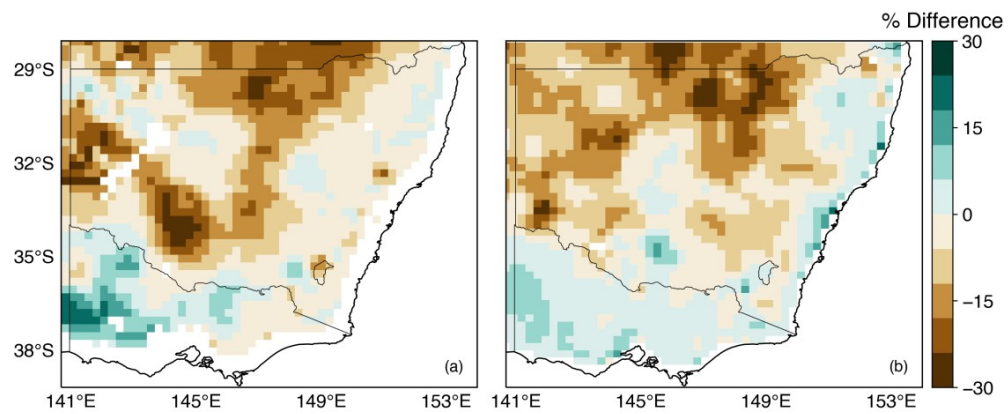


Figure 7: Remotely sensed map of the relative percentage difference between: (a) the mean summer (December–February) vegetation optical depth (VOD) during the Millennium drought (2000–2009) relative to 1993–2000 and (b) the mean summer VOD during the Big Dry (2017–2018) relative to 1993–2016. Note we do not include the final summer 2019 due to the confounding impact of fires across South-East Australia.

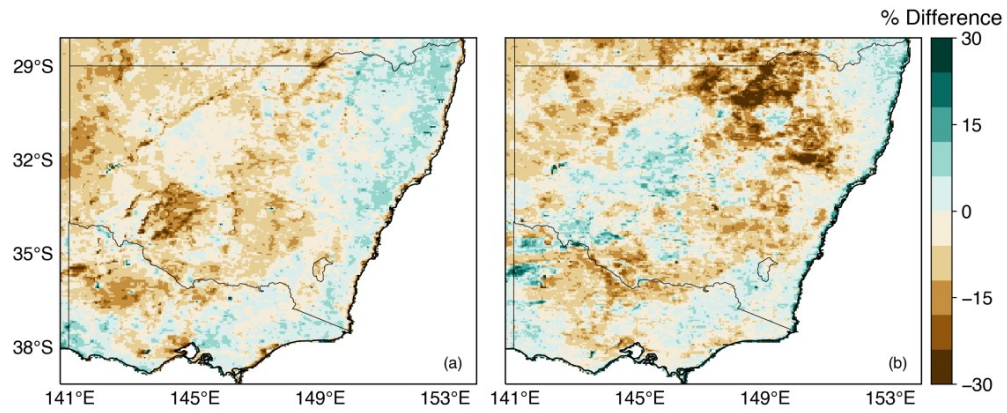
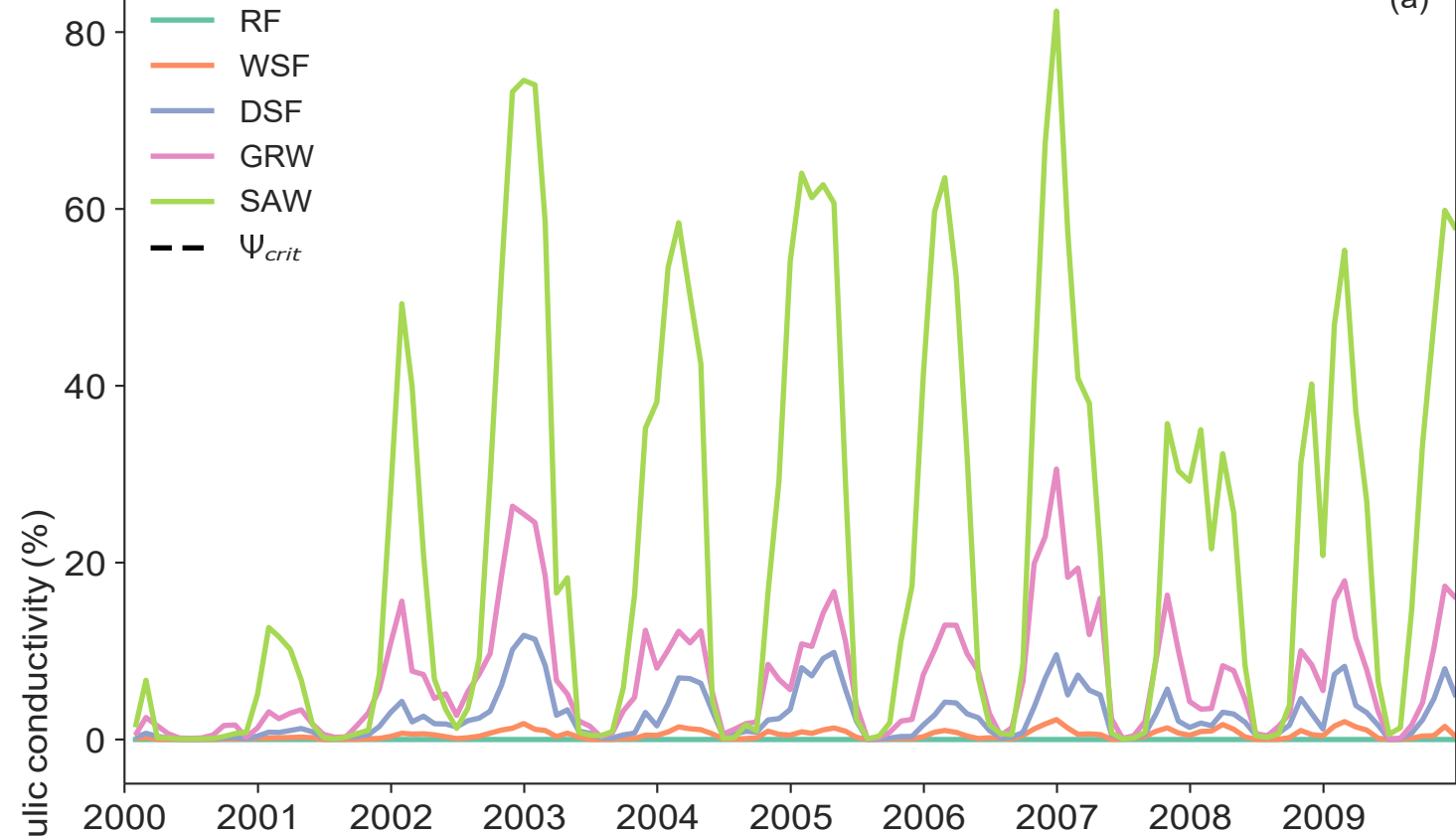
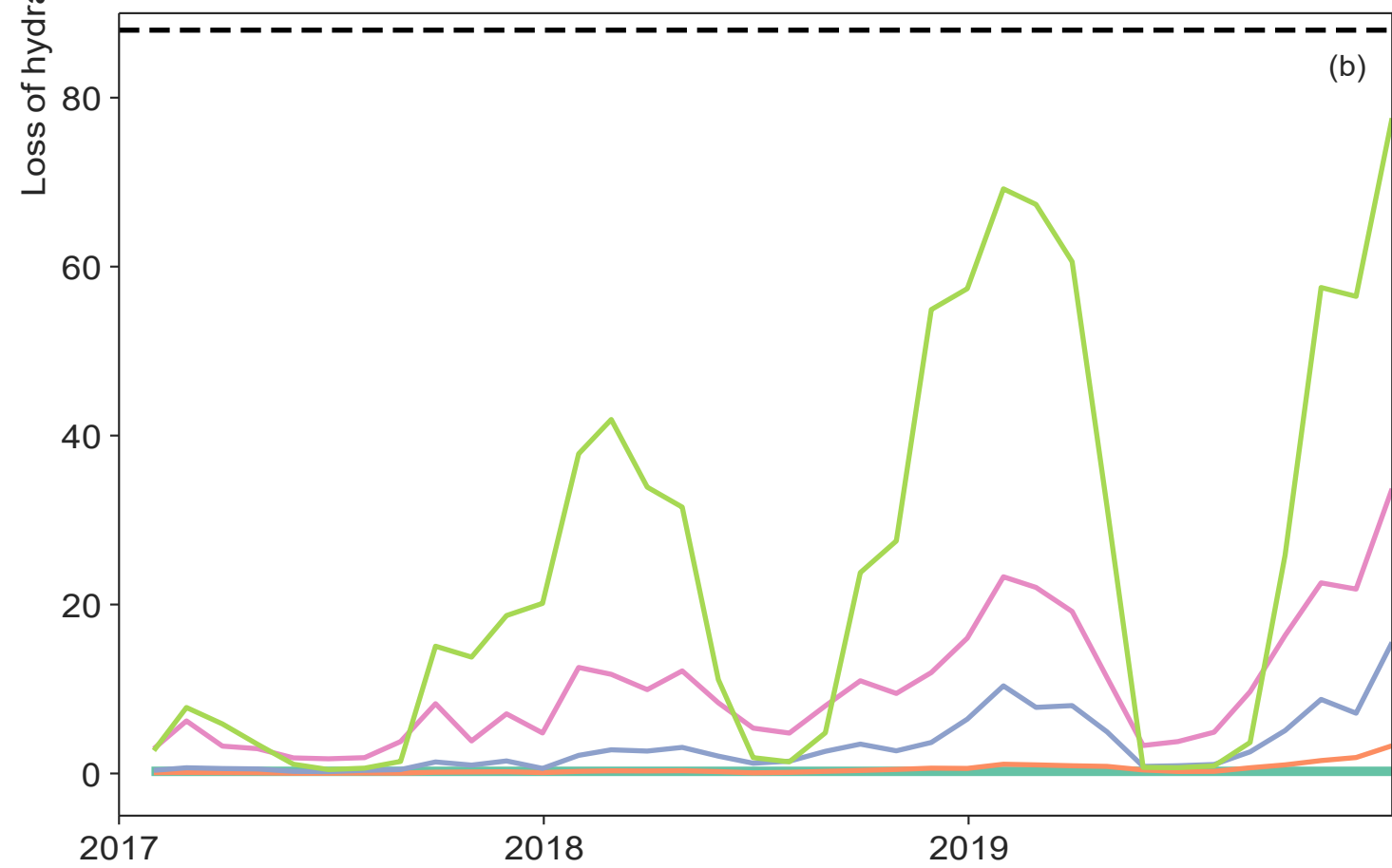


Figure 8: Remotely sensed map of the relative percentage difference between: (a) the mean summer normalised difference vegetation index (NDVI) during the Millennium drought (2000–2009) relative to 1993–2000 and (b) the mean summer NDVI during the Big Dry (2017–2018) relative to 1993–2016. Note we do not include summer 2019 due to the confounding impact of fires across South-East Australia.

(a)



(b)



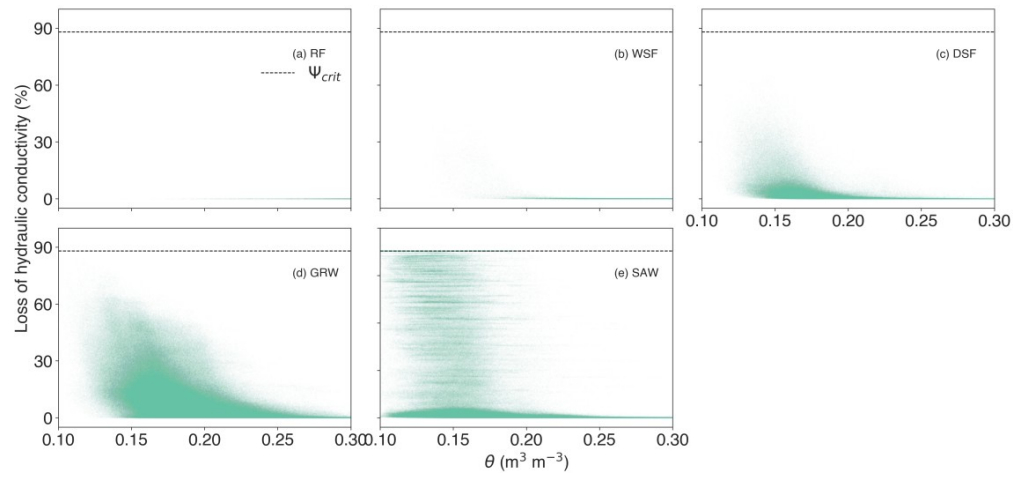


Figure 10: Sensitivity of percentage loss of hydraulic conductivity (%) to soil water availability in the top four soil layers (0.64 m, 80% of roots) for each vegetation class during the Millennium drought. The vegetation classes shown are: Rainforest (RAF), Wet sclerophyll forest (WSF), Dry sclerophyll forest (DSF), Grassy Woodland (GRW) and Semi-arid woodland (SAW). Ψ_{crit} is the xylem pressure inducing a 88 % hydraulic conductivity.

	Definitions	Units	RF	WSF	DSF	GRW	SAW
g_l	Stomatal slope	-	4.2	3.2	4.8	4.8	5.1
g_{min}	Cuticular conductance	mmol	0.25	0.65	0.7	0.65	0.8
V_{cmax}	Value of V_{cmax} at 25 °C	$m^{-2} s^{-1}$ μmol	44.1	84.9	75.6	62.3	92.8
J_{max}	Value of J_{max} at 25 °C	$m^{-2} s^{-1}$ μmol	73.6	141.7	126.3	104.1	154.9
Ψ_f	Reference water potential	$m^{-2} s^{-1}$ MPa	-2	-2.5	-1.7	-3.4	-3.7
S_f	Shape of response to Ψ_l	MPa ⁻¹	2	2	2	2	2
k_{plant}	Plant hydraulic conductance	mmol m^{-2} MPa ⁻¹ leaf s ⁻¹	2.3	1.6	2.4	2.2	2.9
S_{50}	Slope of the percentage loss of hydraulic conductivity	% MPa ⁻¹	74.3	35.3	30.5	26.7	17.8
P_{50}	Water potential at 50% loss of hydraulic conductivity	MPa	-4.3	-3	-3.5	-4.5	-7.1
C_l	Leaf capacitance	mmol $m^{-2} s^{-1}$ MPa ⁻¹	659.1	342.9	349.2	405.1	509.1
C_s	Stem capacitance	mmol $m^{-2} s^{-1}$ MPa ⁻¹	8819.2	53266.1	26255.4	32508.6	11598.5
LA:SA	Leaf area-to-sapwood area ratio	$m^2 m^{-2}$	10000.0	9434.7	7908.6	6139.2	2556.9
WD	Sapwood density	kg m ⁻³	540.0	355.0	460.0	436.7	613.3

Table 1: Summary of vegetation type parameter values. The five vegetation types are: rainforest (RF); wet sclerophyll forest (WSF); dry sclerophyll forest (DSF); grass woodland (GRW); and semiarid woodland (SAW). Values shown are species averages based on Li *et al.* (2018), except for S_f , which was assumed to be fixed and the LA:SA for the RF class which was assumed to be 10,000 $m^2 m^{-2}$.